45. SEDIMENTARY FACIES AND DEPOSITIONAL HISTORY OF THE IBERIA ABYSSAL PLAIN[1]

D. Milkert,[2] B. Alonso,[3] L. Liu,[4] X. Zhao,[5] M. Comas,[6] and E. de Kaenel[4]

ABSTRACT

During Leg 149, a transect of five sites (Sites 897 to 901) was cored across the rifted continental margin off the west coast of Portugal. Lithologic and seismostratigraphical studies, as well as paleomagnetic, calcareous nannofossil, foraminiferal, and dinocyst stratigraphic research, were completed.

The depositional history of the Iberia Abyssal Plain is generally characterized by downslope transport of terrigenous sediments, pelagic sedimentation, and contourite sediments. Sea-level changes and catastrophic events such as slope failure, triggered by earthquakes or oversteepening, are the main factors that have controlled the different sedimentary facies.

We propose five stages for the evolution of the Iberia Abyssal Plain: (1) Upper Cretaceous and lower Tertiary gravitational flows, (2) Eocene pelagic sedimentation, (3) Oligocene and Miocene contourites, (4) a Miocene compressional phase, and (5) Pliocene and Pleistocene turbidite sedimentation. Major input of terrigenous turbidites on the Iberia Abyssal Plain began in the late Pliocene at 2.6 Ma.

INTRODUCTION

Leg 149 drilled a transect of sites (897 to 901) across the rifted margin off Portugal over the ocean/continent transition in the Iberia Abyssal Plain. The Iberia Abyssal Plain lies west of the northern half of the Iberian Peninsula, west and south of Galicia Bank (Laughton et al., 1975). To the north it is connected to the Bay of Biscay via the Theta Gap. An east-west-trending ridge, separated from Tore Seamount by a small channel (Fig. 1), separates the Iberia Abyssal Plain from the Tagus Abyssal Plain to the south. To the east, the adjacent Iberian Margin shows a straight narrow shelf and a steep continental slope. South of 40°N, the slope is cut by several large canyons. Several seamounts (Vigo, Vasco da Gama, and Porto), as well as the larger Galicia Bank (Fig. 1), occur to the northeast of the Iberia Abyssal Plain area.

The Western Iberian Margin

The western Iberian Margin displays two well-differentiated geomorphologic types. North of 39°30'N, the continental slope is dissected by numerous relatively short submarine canyons and gullies that do not reach the abyssal plain. Seaward are several seamounts, including Galicia Bank, Vigo, Vasco da Gama, Porto Seamounts, and other small unnamed ones (Fig. 1). South of 39°N, the continental margin passes smoothly into the upper continental slope, and into a relatively gentle continental rise, which connects with the abyssal plain (Gardner and Kidd, 1987). The major morphological feature is the Nazaré Canyon, south of the Lusitanian Basin. The Iberian continental margin is of special interest because its present morphology has been struc-

tured by both Mesozoic extension and Eocene compression (Pyrenean orogeny) (Boillot et al., 1979), and to a lesser extent by Miocene compression (Betic-Rif phase) (Mougenot et al., 1984).

Previous studies of the Cenozoic geology of the Iberian Margin and this abyssal plain have focused mainly on the processes of rifting and thinning of the continental crust, and on the nature of the ocean/continent transition (Ryan, Hsü, et al., 1973; Groupe Galice, 1979; Boillot, et al., 1980; Mougenot et al., 1985; Mougenot, 1988; Whitmarsh, et al., 1990; Whitmarsh et al., 1993, Masson et al., 1994). These studies have documented that the acoustic basement is formed by Mesozoic sediments, continental basement, and peridotite. Acoustic basement is cut by several faults, forming horst and graben structures that are filled with thin, discontinuous Cenozoic sequences deposited immediately postrift. Rifting began during the Late Triassic, continued in the Late Jurassic, and culminated in breakup during the Early Cretaceous (Wilson et al., 1989). With the exception of Ocean Drilling Program (ODP) Leg 103 (Boillot, Winterer, Meyer, et al., 1987; Comas and Maldonado, 1988), the sediments of the Iberia Abyssal Plain have not been studied in detail. Surface sediments from the plain have been described by Davies (1967), who very cautiously ascribed these sediments to turbidites and pelagic units, but provided no biostratigraphy. Cenozoic deposition was characterized by sediments deposited by a variety of processes, including bottom currents, turbidity currents, and other types of mass-gravity processes.

The western Iberian Margin can be compared with the variety of lithologic and structural features onshore (Fig. 2). Onshore, the northern part of the adjacent Iberian Peninsula contains no Mesozoic or Holocene sediments. A large section of the Hercynian Range crops out with Paleozoic and Precambrian rocks in this region (Ribeiro et al., 1979). On the Iberian Peninsula, the Hercynian Massif consists mainly of folded, thrusted, and metamorphosed rocks of Precambrian and Paleozoic age, extensively intruded by large granitoid batholiths during and after the Hercynian continent-continent collision (Ribeiro et al., 1979). On the shelf, Cretaceous and Cenozoic layers dipping gently west to southwest have a thin veneer of sediments whose precise age is uncertain. The southern part of the Iberian Peninsula consists of low-grade upper Paleozoic metasediments, with an ophiolite marking its northern boundary (Ribeiro et al., 1979). The geometry of the features shown in Figure 2 presents the relationship to the orientation of Hercynian basement structures (Pinheiro et al., this volume).

South of 39°30'N, sediments progressively cover larger areas of the Hercynian terrain in a southerly direction into the basin (Groupe

Galice, 1979). The oldest Mesozoic deposits are Triassic and consist of conglomerates, sandstone, and perhaps evaporites of limnic and lagoonal environments (Hallam, 1971). Lithologies present in the basins adjacent to the Iberia Abyssal Plain (e.g., Lusitanian Basin, Wilson et al., 1989) include Upper Triassic fluviatile sandstones, dolomites, and evaporites; Jurassic shales, siltstones, and sandstones; Cretaceous shallow-marine limestones (Cenomanian to Albian) and fluviatile sandstones (late Aptian to Albian). The Vigo and Porto Seamounts appear to be basement horsts capped by Jurassic carbonates (Groupe Galice, 1979; Mougenot et al., 1984).

Plate Tectonic Setting and Seismicity

Today the Iberian Peninsula is located on the Eurasian Plate, just north of the present-day Africa/Eurasia plate boundary (Grimison and Chen, 1986) The occurrence of earthquakes off the Portuguese margin is well known and is associated with the African/Eurasia lithospheric plate boundary, which lies to the south of the Tagus Abyssal Plain (Martins and Victor, 1990; Fonseca and Long, 1989). Historic records include several major earthquakes (Moreira, 1985), the most important of which was the 1755 Lisbon earthquake, with its epicenter located at Gorringe Bank, about 300 km south-southwest of Lisbon. Earthquakes in the area have been sufficient in number and strength to generate sediment failures that result in turbidity currents.

Oceanographic Conditions

Recent effects of an eastern boundary current along the western margin of Galicia Bank have been mapped by Gardner and Kidd (1987). Currents are produced by the outflow of Mediterranean water, which circulates northward along the Iberian Margin, and appears to influence sediment in depths shallower than 2500 to 3000 m. These currents are capable of forming large-scale sediment waves and drifts along the northwestern Iberian Margin (Kidd, 1982; Kidd and Roberts, 1982; Roberts and Kidd, 1984).

Drilling Objectives and Drill Sites

The principal objective of Leg 149 was to determine the changes in the petrologic and physical nature of the acoustic basement across the ocean/continent transition. The secondary objective was to discover the history of late Cenozoic turbidite sedimentation, to date the deformation of sediments, and to compare this with the Miocene phase of compressional deformation in the Rif-Betic mountains of southern Spain and northern Africa.

The five sites drilled (897 to 901) (Sawyer, Whitmarsh, Klaus et al., 1994) are located along a 120-km, west-east profile in a water depth between 5320 (Site 897) and 4730 m (Site 901) (Figs. 1, 2). All sites were located over basement highs, as required by the principal objective of Leg 149 (Fig. 3). Total sediment recovery comprised about 2400 m of Pleistocene to Upper Jurassic sediments. Figure 3 gives a composite interpreted seismic and sedimentary section through the Leg 149 sites (Sawyer, Whitmarsh, Klaus, et al., 1994).

The sedimentary sequence recovered at the five sites provides the history of the abyssal plain and gives insights into sediment budgets for deposition and reworking throughout the Neogene for the continental margin.

Site 897, the westernmost drill site (Fig. 1), lies over a north-south-trending basement ridge within the ocean/continent transition. The sedimentary sequence recovered at Site 897 (Holes 897A, 897C, and 897D) includes nearly 700 m of Pleistocene to Lower Cretaceous sediments and sedimentary rocks overlying serpentinized peridotite of unknown age (Fig. 3; Shipboard Scientific Party, 1994a).

Site 898 has a similar location, but drilling at that site did not reach the acoustic basement. The stratigraphic sequence consists of 340 m of Pleistocene to upper Oligocene sediments and sedimentary rocks (Fig. 3; Shipboard Scientific Party, 1994b). Very high recover-
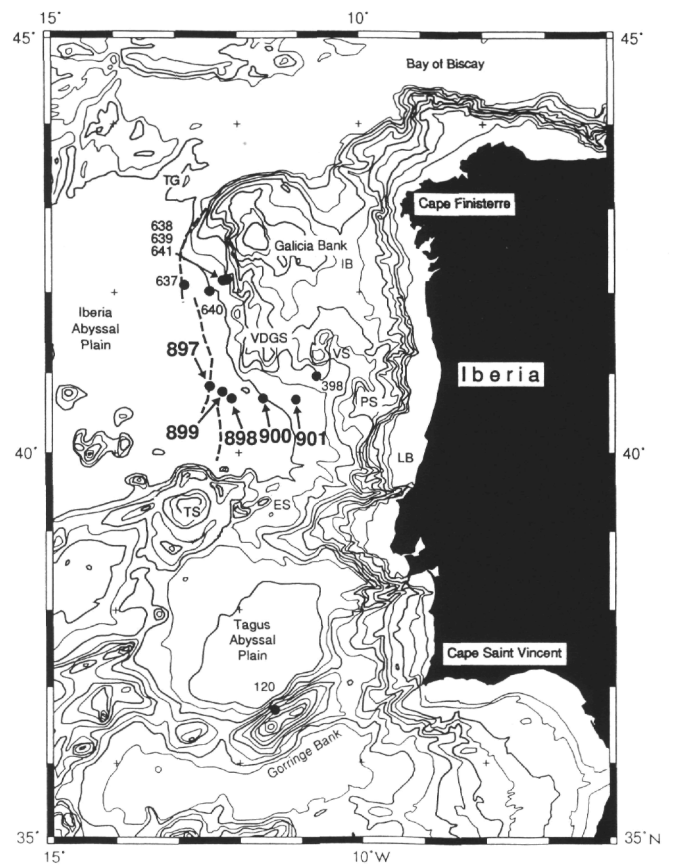
Figure 1. Bathymetry of the west Iberian Margin showing location of Leg 149 Sites 897 to 901 and earlier ODP/DSDP sites (dots). The bold dashed line is the predicted location of the peridotite ridge (Beslier et al., 1993). Labels are as follows: TG = Theta Gap; IB = Galicia Interior Basin; VDGS = Vasco da Gama Seamount; VS = Vigo Seamount; PS = Porto Seamount; LB = Lusitanian Basin; ES = Estremadura Spur; TS = Tore Seamount (modified after Sawyer, Whitmarsh, Klaus, et al., 1994).

ies were achieved by using advanced hydraulic piston coring (APC) down to Core 149-898A-14H in lithologic Unit I, whereas recovery dropped in Unit II, when subsequent drilling was performed with an extended core barrel (XPC).

Site 899 is located on a semielliptical basement high with a steep southern flank. Drilling penetrated a 562.5-m-thick succession, in which all four lithostratigraphic units equivalent to Site 897 were recognized (Fig. 3; Shipboard Scientific Party, 1994c).

Site 900 lies in the transition zone between the continental rise and the abyssal plain. The sedimentary succession at Site 900 penetrated 749 m of an upper turbidite-pelagic sequence (Unit I) and a lower carbonate-rich contourite-turbidite-pelagic sequence (Unit II) (Fig. 3; Shipboard Scientific Party, 1994d). Units III and IV are missing at this site.

Finally, Site 901 is situated within the ocean/continent transition zone over a basement high that appears to be a tilted fault block of thinned continental crust (Sawyer, Whitmarsh, Klaus, et al., 1994; Krawczyk et al., this volume). The upper sedimentary sequence was drilled and washed down to 182 mbsf. Eight meters of sediments were recovered below a thin section of Pliocene nannofossil clay and ooze, apparently unconformably overlying a thin film of Lower Cretaceous clay followed by lower Tithonian black clay, silt, and sandstone (Shipboard Scientific Party, 1994e). These latter two lithostratigraphic sequences could not be correlated with the other sites.
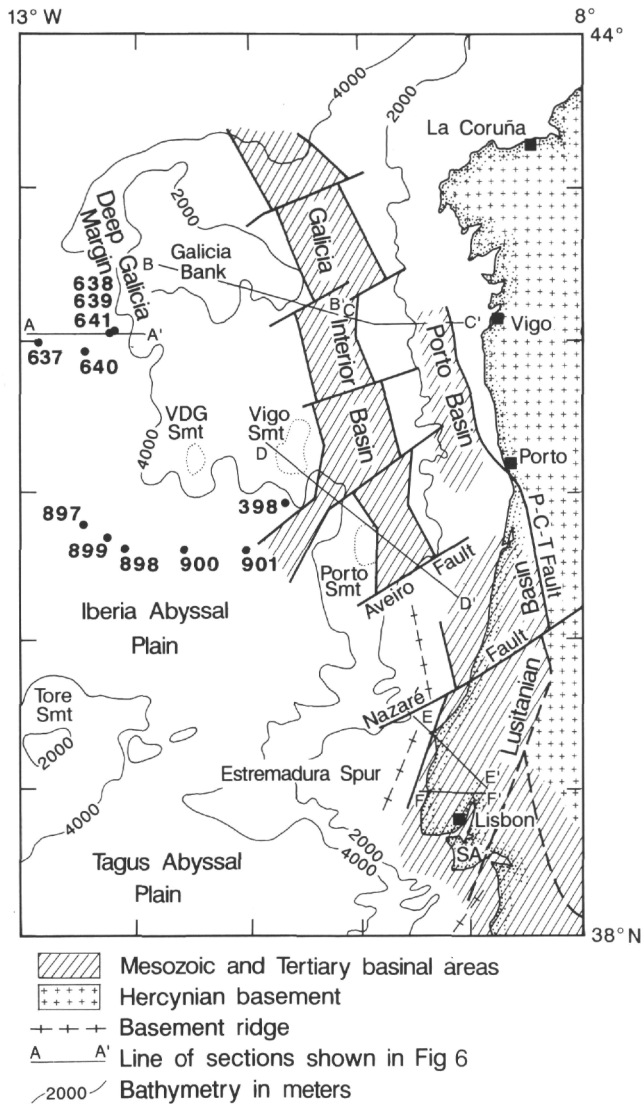
Figure 2. Sketch map showing the distribution of marginal sedimentary basins along the western Iberian Margin. Included are DSDP Site 398, ODP Leg 103 Sites 637 to 641, and ODP Leg 149 Sites 897 to 901 (from Pinheiro, this volume).

AIM AND METHODS

In this synthesis we attempt to consolidate and expand the preliminary interpretations of the Shipboard Scientific Party (Sawyer, Whitmarsh, Klaus, et al., 1994). Integration of revised lithostratigraphic and biostratigraphic interpretations with seismic reflection profiles and core data helps to constrain the sedimentary history since the initial breakup.

Post-cruise research included sedimentological, geochemical, biostratigraphical, and magnetostratigraphic analyses of samples taken from selected intervals of all sedimentary sequences at Sites 897, 898, 899, and 900 (Alonso et al, this volume; Comas et al., this volume; de Kaenel and Villa, this volume; de Kaenel and Bergen, this volume; Gervais, this volume; Gibson et al., this volume; Krawczyk et al., this volume; Kuhnt and Collins, this volume; Liu, this volume; Liu et al., this volume; Marsaglia et al., this volume; McCarthy and Mudie, this volume; Milkert et al., chapter 12, this volume; Pinheiro et al., this volume; Wilson et al., this volume; Zhao et al., this volume). The sampling interval was determined according to the thickness and variations of individual beds.

LITHOSTRATIGRAPHIC SEQUENCE

According to Sawyer, Whitmarsh, Klaus, et al. (1994), the lithostratigraphic succession could be subdivided into four lithostratigraphic units on the basis of changes in lithology and the degree of lithification.

The regional stratigraphic correlation between lithologic Units I and II is shown in Figure 4 (Sawyer, Whitmarsh, Klaus, et al., 1994). At Sites 897 through to 900, the lithostratigraphy consists of an upper turbidite-pelagic sequence (Unit I and Subunit II A) and a lower contourite-turbidite-pelagic sequence (Subunit II B) with a decreased carbonate content. The two sequences contrast sharply in terms of evidence of reworking by contour currents (which are present only in the lower sequence) and in the abundance of siliceous allochems (virtually absent in the upper sequence) (Sawyer, Whitmarsh, Klaus, et al., 1994).

The two lithostratigraphic sequences recovered at Site 901, consisting of a thin film of Lower Cretaceous clay followed by lower Tithonian black clay, silt, and sandstone (Shipboard Scientific Party, 1994e), could not be correlated with the other sites.

Unit I

Unit I is characterized by terrigenous turbidites, the product of turbidity current deposition on an abyssal plain, and pelagic sediments. Pleistocene to Pliocene terrigenous turbidite sequences (Unit I) comprise 292 m at Site 897 and 163 m at Site 898. Their lithologies are described in detail by Milkert et al. (this volume). Only 22 m of Unit I terrigenous turbidites and pelagic sediments were recovered at Hole 899A because the hole was washed down to 82 m. Unit I at Site 900, although containing both turbiditic and pelagic facies, shows little siliciclastic sand in comparison to its counterparts at Sites 897, 898, and 899. At Site 900, the unit is divided into three Subunits. Subunits IA and IC contain turbiditic and pelagic sediments, and are separated by the pelagic nannofossil clays and oozes that comprise Subunit IB (Shipboard Scientific Party, 1994d).

Unit II

Major lithologies in Unit II comprise calcareous claystones, claystones, silty claystones, siltstones, and sandstones. They reflect deposition on an abyssal plain setting and reworking by contour currents. The lower Pliocene to middle Eocene Unit II at Site 897 consists of 328 m of muddy turbidites and calcareous contourites. Here, Unit II was subdivided into three Subunits on the basis of color and the proportion of claystone vs. coarser-grained lithologies (Sawyer, Whitmarsh, Klaus, et al., 1994).

At Site 898, lithologic Unit II comprises 177 m of middle Miocene to upper Oligocene sediments and is divided into two Subunits. Subunit IIA shows homogeneous clay lithologies, whereas Subunit IIB, with its upward-darkening alternations of carbonate-rich and relatively carbonate-poor sediments containing biogenic siliceous material, contrasts with the clearly turbidite-related lithologic association of Unit I. This unit seems to be a combination of possible turbidites and contourites such as the ones described by Stow and Piper (1984). At Site 899, the sedimentary sequences of this unit consist of 211 m of lower Pliocene to upper Eocene calcareous claystones, claystones, silty claystones, siltstones, and sandstones. Subunit IIA (early Pliocene to middle Miocene) consists of intensely bioturbated brown claystone with scattered turbidites. Subunit IIB is dominated by greenish gray upward-darkening sequences with basal fine sandstone beds. The tops often show "lag deposits" or large foraminiferal tests. All these features point to reworking by contour currents, as described by Stow and Piper (1984); a few mud turbidites are intercalated (Sawyer, Whitmarsh, Klaus, et al., 1994).

At Site 900, Unit II is dominated by claystone, claystone with silt/silty claystone, nannofossil claystone, and nannofossil chalk. Fora-

687
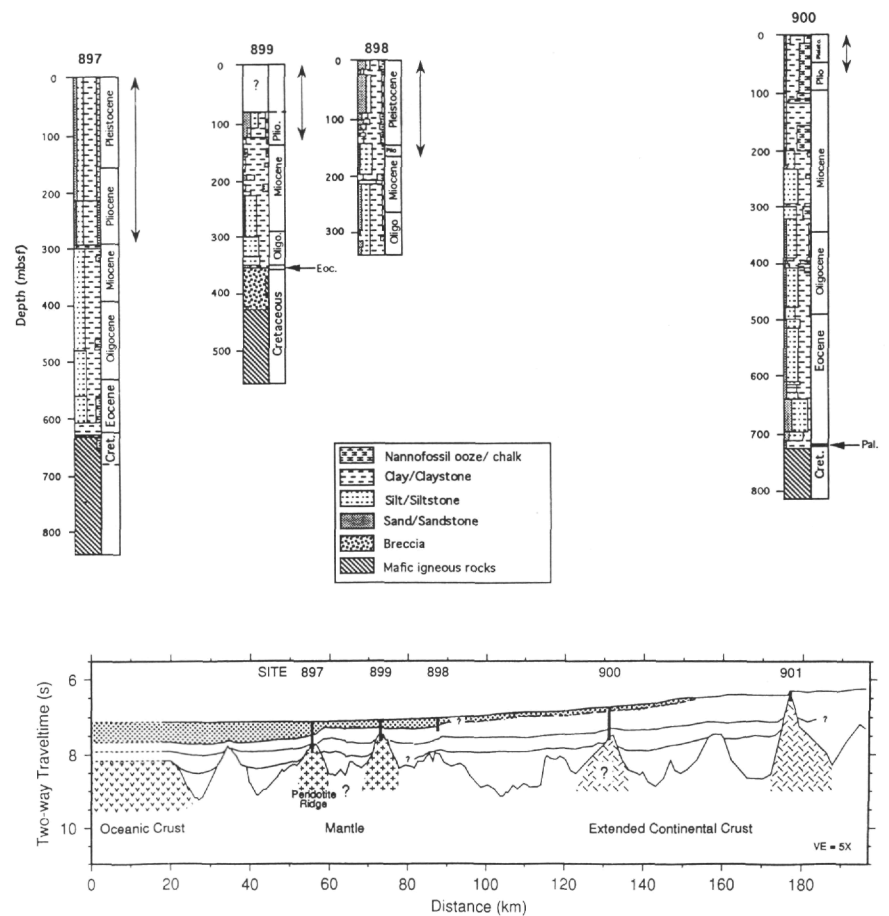
Figure 3. Summary of lithologic columns for Sites 897 to 900 and a composite interpreted seismic section through these sites (see Fig. 1). Shading in the seismic section indicates the distribution of Pleistocene and Pliocene terrigenous turbidites and pelagics (Subunit IA) in the lithologic column (Sites 897 to 900) (modified after Sawyer, Whitmarsh, Klaus, et al., 1994).

minifer-rich sandstones and calcarenites occur as a distinctive minor lithology in Subunit IIA and form as much as 20% to 30% in some cores in Subunit IIB, where they are often cemented by calcite. Both contain upward-darkening sequences and are interpreted as deposits of turbidity flows and contour currents.

Unit III

Unit III is mainly siliciclastic in composition and occurs at Sites 897 and 899. It reaches a total thickness of 30 m at Site 897 and around 10 m at Site 899. The unit was divided into two Subunits. Subunit III A at both sites is composed entirely of brown terrigenous clays that are of latest Maastrichtian-early Eocene age (Kuhnt and Collins, this volume). Subunit IIIA is interpreted as the product of slow accumulation of clay in an oxygenated environment. The clay and fine silt are most likely continental material supplied by low-density turbidity flows or by the nepheloid layer of contour currents. At Site 897, Subunit IIIB is characterized by upward-fining sequences of carbonate pebbles and gravel conglomerates, coarse sandstones, sandstones, and silty claystones of Aptian age (de Kaenel and Bergen, this volume). Lithologies in Subunit IIIB at Site 899 show great variability, and include variegated sandstone, white highly altered volcanic ash, laminated brown claystone, lighter colored silty claystone with black concretions, and poorly cemented, multicolored, polymictic, clayey conglomerate. Highly altered basaltic clasts are present in the gravel- and sand-sized fractions. The highly variegated conglomerates (Subunit IIIB) are of Campanian/late Maastrichtian (Gervais, this volume) to middle/late Eocene age (Kuhnt and Collins, this volume). This Subunit is interpreted as a mixture of fine-grained pelagic deposits and high-density turbidity currents or fluidized sand-silt-clay debris flows that developed on relatively gentle slopes.

Unit IV

The late Aptian to late Hauterivian age Unit IV (de Kaenel and Bergen, this volume) comprised a maximum of 38 m (Hole 897D) of serpentinized peridotite between intervals of siliciclastic and carbonate lithologies (Fig. 5) and directly overlies acoustic basement.

At Site 899 Unit IV comprised 188.2 m of an unusual sequence of rocks with three different lithologies: (1) three serpentinite breccias that range in thickness from nearly 100 (upper breccia) to less than 10 m (middle and lower breccia), described in further detail by Shipboard Scientific Party, 1994c, Comas et al. (this volume), and Gibson et al. (this volume); (2) an association of claystones, calcareous claystones, soft, altered, and deformed serpentine masses, and minor siltstone is intercalated between the breccia intervals and sections of serpentinized ultramafic rocks; and (3) discrete sections of unbrecciated serpentinite, serpentinized peridotite, gabbro and basalt fragments. The basalt fragments are of variable composition and some occur within the claystones and the soft, altered, and deformed serpentine masses. The breccia units are poorly sorted and are composed of ultramafic clasts of a restricted compositional range.

At Site 897, no unit clearly analogous to the serpentinite breccia at Site 899 is well developed. Nevertheless, certain broad similarities can be identified between lithologic associations in Unit IV. Serpentinized peridotite, ranging from 15 cm to 1.5 m thick, is sandwiched between dark-green claystone and a variety of other lithologies, including various breccias at Site 897 (Shipboard Scientific Party, 1994a). Sedimentary intervals yield ages that young upwards and range from late Hauterivian to early Aptian. Deposition at this site occurred at the foot of a fault escarpment that exposed serpentinized peridotite basement during the Early Cretaceous.
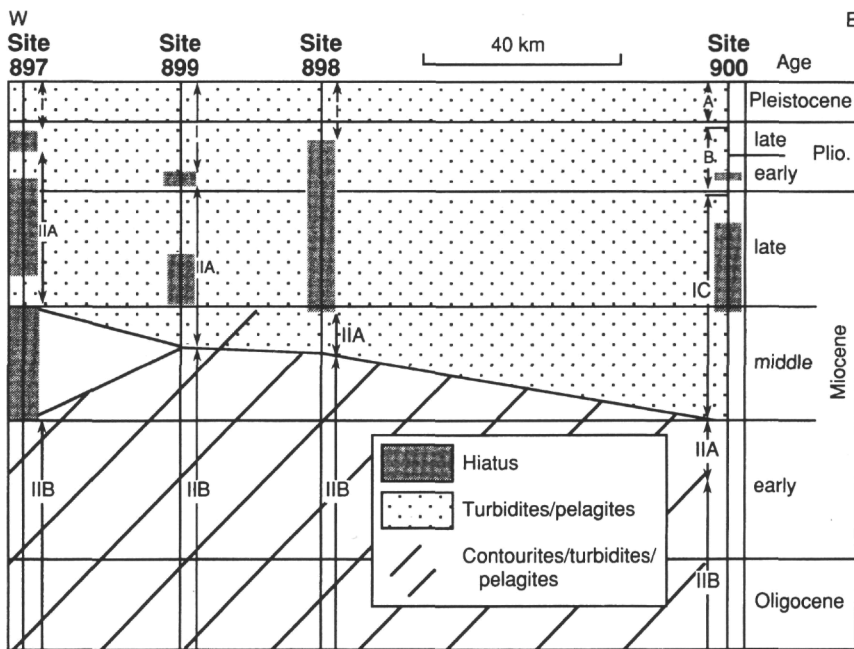
Figure 4. Regional stratigraphic correlation chart for lithologic Unit I and Subunit IIA at Sites 897 to 900. The contourite-turbidite-pelagic sequence contains abundant siliceous allochems and reworked carbonate grains. The turbidite pelagic sequence shows no evidence of reworking by contour currents (from Sawyer, Whitmarsh, Klaus, et al., 1994).

FACIES TYPES AND ASSOCIATION

Pelagic Sediments

Pelagic clays, marls, and oozes are present in lithologic Units I and II. At this water depth, the proportion of calcium carbonate varies cyclically, in relation to the variation in bottom-water composition, a well-known phenomenon that occurs in other North Atlantic basins (Weaver and Kuijpers, 1983; Raymo et al., 1987). Pelagic layers vary in thickness between 0.01 and 1.89 m, with the thickest pelagic units being observed at Site 900. The pelagic sediment contains an average of 45% $CaCO_3$ and 0.31% organic carbon (Milkert et al., this volume). Pelagic sediments show slight to moderate mottling caused by bioturbation, but no distinct ichnofauna is visible. Bioturbation continues downward from the pelagic sediments into the tops of the underlying turbidites.

Brownish red, pelagic clays are common during the Eocene and Paleocene in lithologic Subunit IIIA at Sites 897 and 899; during this time interval, the regional carbonate compensation depth (CCD) was relatively shallow (Emery and Uchupi, 1984). The clay shows vague color banding, and bioturbation is not apparent. The claystones at Site 899 contain several black, organic-rich layers (Sawyer, Whitmarsh, Klaus, et al., 1994), and brownish black concretions, which are barren.

Turbidites

Pleistocene and Pliocene sedimentation at Sites 897, 898, 899, and 900 is dominated by deposition of terrigenous turbidites, separated by thin pelagic layers (Fig. 6). Turbidite sequences are easily distinguished from pelagic sediments by their graded bases, distinctive darker colors, and usual lack of bioturbation (Sawyer, Whitmarsh, Klaus, et al., 1994; Milkert et al., this volume). The base of each turbidite is clearly defined as a sharp boundary over mottled, lighter colored pelagic sediment. The structureless-to-laminated basal sand and silt layers in the turbidites correspond to the T_{c-d} division of Bouma (1962); the T_{a-b} interval is absent. Clay-rich intervals are bioturbated to laminated, and contain significant amounts of reworked nannofossils, and correspond to the turbiditic mud divisions (T_{e1-e3}) of Stow and Piper (1984). Visually distinguishing the T_e facies from the pelagic interval is difficult in areas where fine-grained pelagic sediments are mixed downwards by bioturbation and drilling disturbance.

A huge number of turbidites was deposited in the last 2 million years. A maximum of 48 turbidites (4 to 60 cm thick) was recognized in a single 9.5-m core (Core 149-898A-14H). In general, the frequency of turbidites varies from 2 to 7 per meter throughout the different cores. The large number of turbidites (e.g., 600 in Hole 898A) makes it difficult to correlate individual turbidites between sites (Milkert et al., this volume).

The terrigenous turbidites appeared very similar throughout the sedimentary sequence during shipboard description. More detailed post-cruise examination and additional visual core descriptions allowed a separation of these turbidites into four groups on the basis of different color and lithologic composition (Milkert et al., this volume).

Four different types of turbidite can be determined on the basis of color, carbonate, and organic carbon content:

Type 1. Turbidites with gray terrigenous/siliceous and mica-rich bases.

Type 2. Gray, calcareous, terrigenous turbidites with sandy, silty bases.

Type 3. Calcareous turbidites with foraminifer-rich bases.

Type 4. Lower Pleistocene brownish red sandy turbidites, which are common at all sites.

Despite these visual differences, analysis of major and minor elements by inductively coupled plasma atomic emission spectroscopy (ICP-AES) shows a very similar composition for all turbidites (Milkert et al., this volume). The turbidites originate mainly from continental erosion. In general, the Iberia Abyssal Plain turbidites have low Fe, Mg, Ti, and Zr contents with high proportions of Al and alkali metals. This indicates a continental provenance for the aluminosilicate phases and confirms a continental source region, similar to the element distribution described for organic-rich turbidites on the Madeira Abyssal Plain by DeLange et al. (1987). It probably indicates a uniform composition throughout the continental source area, rather than a single source for the Iberia Abyssal Plain turbidites.

Contourites

Contourite facies and mixed contourite/pelagic facies are common throughout the entire Miocene and Oligocene at Sites 897, 898, 899, and 900.

The distinction between turbidites and contourites is difficult to make, especially when bottom currents modify deposits containing
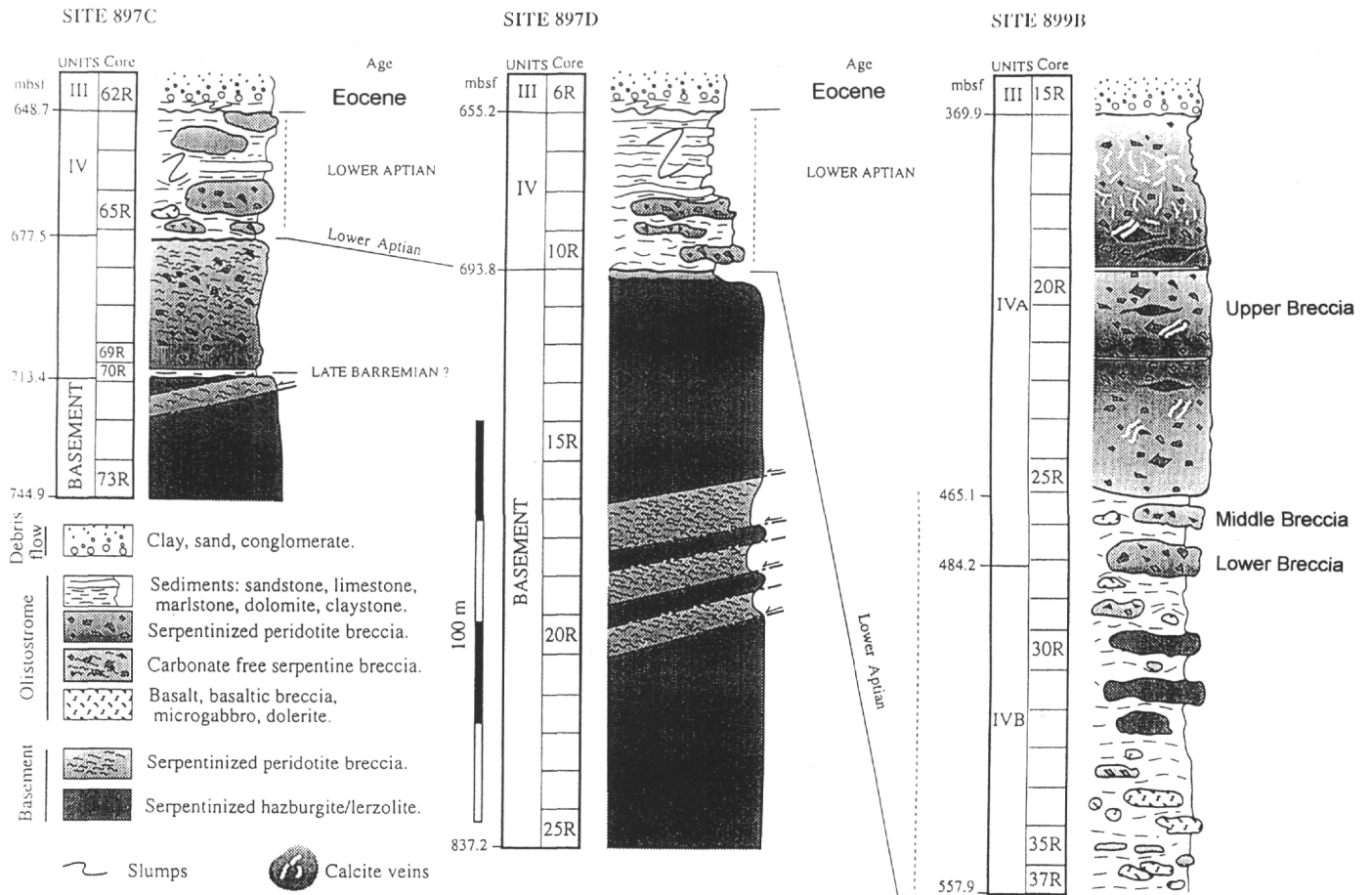
Figure 5. Lithologic sequences of Eocene to Aptian gravity-flow sediments at Sites 897 and 899. The artwork shows sampled lithologies and core, but it is not related to recovered core intervals. The boundaries of Units III and IV are located after Sawyer, Whitmarsh, Klaus et al. (1994). Sediments in Core 149-897C-70R indicate top of acoustic basement at 713.4 mbsf. Because of a generalized drawing, veining in the smaller breccia bodies is not shown. Datum at the bottom of Unit III (modified after Comas et al., this volume).

turbidites (Faugères and Stow, 1993). Despite these problems, evidence of occasional bottom-current activity was found in several sandy layers that have low pelite content and contain high concentrations of coarse foraminiferal tests (Alonso et al., this volume). Comas and Maldonado (1988) described similar foraminiferal sands in the Iberia Abyssal Plain, and Faugères et al. (1984) obtained comparable pure foraminiferal contourite sands in several North Atlantic basins and hypothesize that these deposits seem to be winnowed concentrations formed by normal bottom currents.

In addition to sandy sediments in the Iberia Abyssal Plain, silty sediments of mixed biogenic/terrigenous or only biogenic composition were recognized throughout lithologic Subunit IIB at all Leg 149 sites (Alonso et al, this volume). Silty sediments of this type could be recognized (Fig. 7; Sawyer, Whitmarsh, Klaus, et al., 1994). These deposits could be attributed to the effect of bottom-current processes. Silty deposits are differentiated from the T_d division turbidites on the basis of their bimodal or polymodal grain size distribution in the total cumulative curve, the lack of vertical grading, and the poor preservation of nannoplankton.

Therefore, Alonso et al. (this volume) and the Shipboard Scientific Party (Sawyer, Whitmarsh, Klaus, et al., 1994) distinguished two types of contourite facies:

1. Sandy contourites (Fig. 7) consist of poorly sorted silty sands, largely composed of planktonic foraminifers with uniformly high carbonate content, that result from a combination of reworking and deposition from bottom current activity.

2. Silty contourites (Fig. 8) result from the depositional action of bottom currents (Stow and Piper, 1984) and can be subdivided, on the basis of sand composition and carbonate content, into calcareous sandy, calcareous silty, and terrigenous, silty contourites as shown in Table 1 and Figure 8.

Slumps and Slides

Slumps and slides are present within several single cores in the Pleistocene and Pliocene section. A 1.3-m-thick debris flow occurred in the early Pliocene (Section 149-897C-22R-03, Zone NN18 after Liu et al., this volume; Zone N20/N19 after Gervais, this volume). It reveals a highly folded and scrambled mixture of pelagic oozes and silty sands with a small amount of turbidite clay. An inverted, 83-cm-thick sequence, containing three single turbidites, was obtained from Section 149-898A-12H-01. It is underlain by an unusual, greater than 1-m-thick, homogeneous turbidite mud. This flow is of late Pleistocene age (Zone NN19 after Liu et al., this volume or Zone N23/N22 after Gervais, this volume). This section is interpreted as a single block, which was overturned by a gravity flow. The above-described structures cannot be correlated between the drill sites, suggesting that they originated from different events that did not reach the other locations.
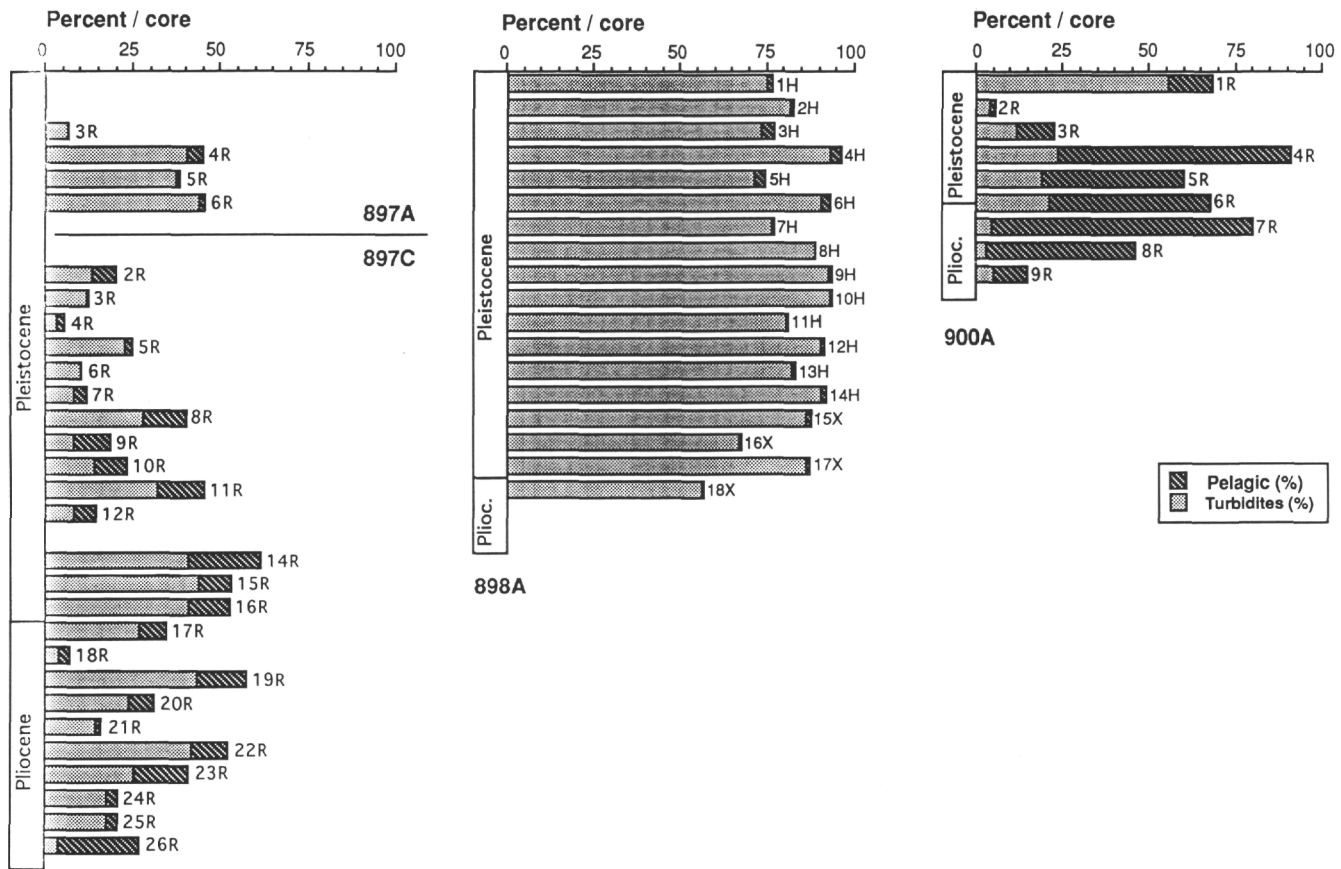
Figure 6. Percentage of turbidites and pelagic sediments through lithologic Subunit IA at Sites 897, 898, and 900. The percentage recovery is expressed as a percentage of the recovered material in the cores.

Slump and slide structures are equally common in lithologic Subunit IIB, mainly at Hole 899B (e.g., intervals 149-899B-3R-4, 85-110 cm; 5R-3, 30-80 cm; 7R-4, 90-95 cm; 8R-3, 100-145 cm; Shipboard Scientific Party, 1994c). Small slump folds are formed in nannofossil claystone and silty claystone.

Conglomerates

In Holes 897C and 897D, Subunit IIIB consists of gravity-flow deposits of poorly sorted, poorly cemented granule-to-pebble clayey conglomerate that grades upward to granule conglomerate and very coarse-grained, lithic, ferruginous clayey sandstone. This upward-fining sequence occurred over an interval of approximately 20 m in Hole 897C and in excess of 10 m in Hole 897D; the sequence was dark-reddish and variegated in both holes (Sawyer, Whitmarsh, Klaus, et al., 1994). Resedimented clasts included in the conglomerates have diverse lithologies and facies: white limestone, micritic limestone, marlstones, dolomite, and varied turbiditic arkosic-to-lithic sandstones. Minor clasts of shallow-water carbonates included in the conglomerates of Subunit IIIB are interpreted as being deposited from high-concentration sediment flows that were transported by high-density turbidity currents or as fluidized sand-silt-clay debris flows on relatively gentle slopes (Shipboard Scientific Party, 1994a). The basal, poorly sorted, conglomerate/gravel interval can be considered as a deposit from a single debris flow. Clasts and granules of basalt and serpentinized peridotite are present as minor components in the conglomerate and coarse sandstone. Samples at the base of this conglomerate yield an early late Eocene age (de Kaenel and Bergen, this volume).

At Site 899, reddish variegated ferruginous conglomerate and coarse sandstone, including basalt pebbles, were sampled in one interval of about 1 m within Subunit IIIB (Shipboard Scientific Party, 1994c). The Subunit IIIB lithologies at Site 899 are dated as middle to late Eocene by Kuhnt and Collins (this volume), using benthic foraminifers, or as Eocene by Gervais (this volume), using planktonic foraminifers (Fig. 3).

Breccia Deposits

In lithologic Unit IV blocks and clasts of serpentinized peridotite were recovered at Site 897 (Shipboard Scientific Party, 1994a) and Site 899 (Shipboard Scientific Party, 1994c). At Site 899, three serpentinite breccias were recovered that contain peridotite blocks and intercalated Lower Cretaceous claystones and siltstones, clasts of basalt, microgabbro, and mylonite. These unusual breccia deposits from Site 899 did not have an obvious equivalent at Site 897. The mechanism of deposition of these blocks was discussed by Comas et al. (this volume) and Gibson et al. (this volume).

Comas et al. (this volume) examined the origin of the Lower Cretaceous deposits recovered at Sites 897 and 899, which were included in lithologic Unit IV (Sawyer, Whitmarsh, Klaus, et al., 1994), and considered the serpentinized peridotite breccia at Site 899 to be a tectonic cataclasite. The igneous-sedimentary complex at both sites is interpreted as an olistostrome, and breccia intervals are interpreted as olistoliths or blocks from cataclastic breccias. The terms "olistostrome" or "gravitational mélange" are widely used in the Alpine and Tethys literature (Abate, et al. 1970; Einsele, 1992) and describe thick, stratiform, heterogeneous, more or less chaotic, deposits that
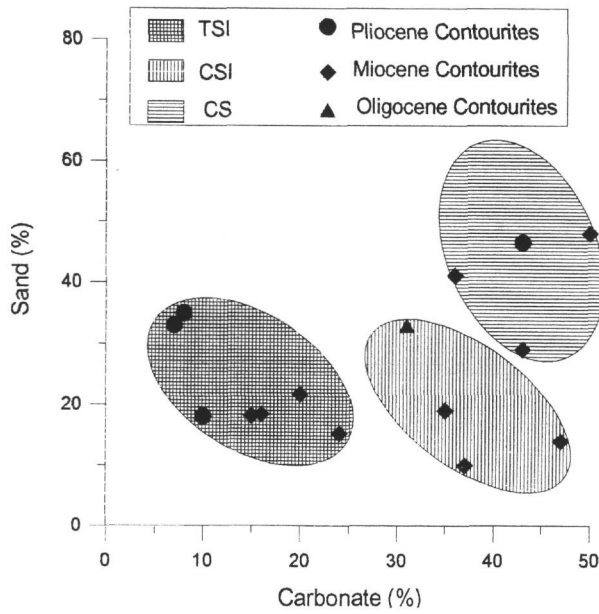
Figure 7. Sand content vs. carbonate content for Pliocene to Oligocene contourites from Sites 897, 898, and 900 showing differentiation of terrigenous silty (TSI), calcareous silty (CSI), and calcareous (CS) contourites.

occur over wide areas and that accumulated as a result of tectonically induced massive gravitational sliding in various tectonic settings. These units can contain large blocks up to several hundred meters in thickness and can travel long distances.

The Leg 149 olistostrome, involving sedimentary, ultramafic and mafic rocks, is thought to be derived from a lower Aptian ridge related to an inferred transform fault boundary between the Galicia Bank margin and the Iberia Abyssal Plain at this time Figueiro Fault Zone (Whitmarsh et al, 1990). Cataclastic breccias and other fault rocks (basalt and gabbro), which form part of the olistostrome, mainly originated from wrench tectonics in the transform fault zone. Activity on the Figueiro Fault Zone occurred only during the development period for transitional crust and early stages of seafloor spreading in the Iberia Abyssal Plain (from approximately late Hauterivian, 129 Ma, after Gradstein et al., 1994) and terminated at the time of break-up on the Galicia Bank margin (latest Aptian-early Aptian, approximately 114 Ma).

Comas et al. (this volume) support the idea that the olistostrome originated at an active major fault far away from the drilling area and outside the ocean/continent transition because of the basin plain character of the early Aptian sedimentary environment at both Sites 897 and 899. The Aptian olistostrome was cored on discrete fault-bounded basement highs at Sites 897 and 899 (Sawyer, Whitmarsh, Klaus, et al., 1994). Comas et al. (this volume) suggest that these gravity slide deposits were originally deposited on a flat basin-plain environment and were uplifted during the postrift stage of the west Iberian Margin. The "long-distance transport" of the olistostrome is expressed by internal deformation, and by the roundness and alteration of the involved clasts. Strong affinities are present between the sedimentary facies involved in the olistostrome, the sediments drilled during Leg 103 at ODP Site 638 (Boillot Winterer, Meyer, et al., 1987), and a similar facies at DSDP Site 398 (Shipboard Scientific Party, 1979). Correlations were made between metabasite and gabbro clasts in the olistostrome and chlorite-bearing schists sampled on top of the peridotite in the Galicia Bank margin (Boillot et al, 1988; Beslier et al., 1993).

The hypothesis of Comas et al. (this volume) emphasizes the role of the Figueiro Fault Zone (Whitmarsh et al, 1990) as a major tectonic lineament during the Aptian. The reality of this fault zone is a mat-
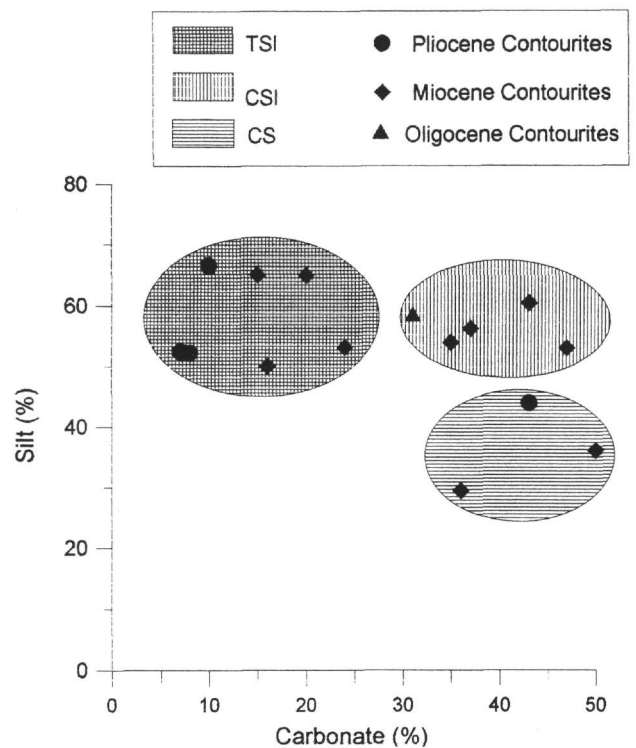
Figure 8. Silt content vs. carbonate content for Pliocene to Oligocene contourites from Sites 897, 898, and 900 showing differentiation of terrigenous silty (TSI), calcareous silty (CSI), and calcareous (CS) contourites.

Table 1. Variations of types of contourites.

	Calcareous sandy (CS)	Calcareous silty (SI)	Terrigenous silty (TSI)
Pleistocene			
Pliocene	X		X
Miocene	X	X	X
Oligocene			X

ter of discussion because of its weak signature on seismic profiles (Beslier et al, 1993). The present-day seismic signature from the paleotransform fault may be masked either by a later transtensional situation or by post-Aptian faulting of the western Iberian Margin (Comas et al., this volume).

Gibson et al. (this volume) interpret the lower Aptian serpentinite breccia unit at Site 899 as being a giant submarine landslide, generated by slope failure on a large, nearby serpentinite fault scarp. Their interpretation focuses on the breccia unit at Site 899. Giant landslides are a typical feature of regions undergoing rapid extensional deformation (Bonatti et al., 1973; Bonatti et al., 1974; Bernoulli and Weissert, 1985). It is proposed that the basement topography at the time of formation of the serpentinite unit differed significantly from the present topography buried beneath the Iberia Abyssal Plain, and, as a result, the location of the source serpentinite escarpment is unknown. The authors indicate that the source was likely to have been within several kilometers of Site 899.

Gibson et al. (this volume) discuss the following possibilities for the mechanism of formation of the breccia units: in situ brecciation, formation in cataclastic shear zones, diapiric extrusion, and massflow deposits. They conclude that the breccia units at Site 899 show many similarities to subaerial landslides and associated rock avalanche deposits (Watson and Wright, 1969; Siebert, 1984; Stoopes

Table 2. Paleomagnetic and biostratigraphic datums at Sites 897, 898, and 900 (from Zhao et al., this volume).

Magnetic datum (Chron or subchron)	Biostratigraphic datums (N, F)	Age (Ma) (magnetism)	Age (Ma) (biostrat.)	Site 897 Depth range (mbsf) (magnetism)	Site 897 Depth range (mbsf) (biostrat.)	Site 898 Depth range (mbsf) (magnetism)	Site 898 Depth range (mbsf) (biostrat.)	Site 900 Depth range (mbsf) (magnetism.)	Site 900 Depth range (mbsf) (biostrat.)
Brunhes/Matuyama	NN19h,N23	0.78	0.48–0.83	108.2	50.35–109.26	29.06	20.34–47.20		
Jaramillo	NN19f	0.99–1.07	0.89–1.06	128.72–137.4	127.5–137.2	54.69–59.77	54.69–59.77	21.08	21.76–26.62
Olduvai	NN19a,N22	1.77–1.95	1.66–1.91	198.2–207.33	181.18–207.17	144.33–163.18	144.33–163.18	47.00–48.06	43.86–47.96
Reunion?	NN18	2.14–2.15	1.95–2.36	234.14–235.66	107.87–263.83		196.7–206.4		
Matuyama/Gauss	NN16	2.58		292.88	292.43			64.55	64.95–79.29
Mammoth		3.22–3.33						76.9–78.7	
Gauss/Gilbert	NN15/N19	3.58						79.19	
Cochiti		4.18–4.29						84.2–84.4	
Nunivak		4.48–4.89						87.1–87.5	
Sidutjall		4.8–4.89						89.3–90.0	
Thvera		4.98–5.23						95.2–95.6	
C3An.1n		5.83–6.05						113.8–114.6	
C3An.2n		6.17–6.45						115.4–115.8	
C3Bn		6.79–6.94						121.9–124.2	
C3Br.1n		6.98–7.02						126.8–127.2	
C3Br.2n		7.18–7.22						132.3–132.7	
C4n.1n		7.27–7.4						134.3–136.2	
C4n.2n		7.48–7.9						138.3–140.5	
C4r.1n		8.06–8.09						144.9–?	
C5D?	N7/N6	17.31–17.65	e. Miocene			197.03–206.4	196.7–206.4		

and Sheridan, 1992; Yarnold, 1993). These similarities include the presence of angular fragments with jigsaw/crackle texture; a general lack of sorting, compatible with very rapid, essentially instantaneous formation, but with larger boulders occurring near the upper surface of the units; a matrix generated by fragmentation of the clasts and a size continuum between the clasts and the matrix; and internal deformation zones or slip zones. Observations at Site 899 and the general stratigraphic framework for Unit IV (Shipboard Scientific Party, 1994c) show that the serpentinite breccias are interbedded with sedimentary units. Biostratigraphic ages suggest a normal stratigraphic succession (de Kaenel and Bergen, this volume) and, therefore, the breccias are most simply interpreted as normal bedded units. The source for the serpentinite breccias was presumably a nearby fault scarp exposing massive serpentinite, but Gibson et al. (this volume) do not provide any distance relations.

Wilson et al. (this volume) could find no indications from seismic profiles to suggest that basement topography established during rifting was modified by later deformation. Seismostratigraphic unit 6 of Wilson et al. (this volume) is of Aptian to possible Valanginian age, which increases the difficulty of interpreting the setting of the Aptian debris flows and rock-fall breccias encountered on the crest of basement highs at Sites 897 and 899. There is no evidence for the basement ridge at Site 897 being tectonically uplifted or rising diapirically during deposition of the seismostratigraphic units 1 to 5. This conclusion contradicts suggestions made by Comas et al. (this volume) and Gibson et al. (this volume) that the basement topography that existed at the time of formation of the Aptian olistostromes at Sites 897 and 899 differed significantly from that observed today (see also Whitmarsh and Sawyer, this volume). Debris-flow deposits, such as those occurring in lithologic Subunits IVA and Subunit IVB at Site 899 (Shipboard Scientific Party, 1994a, c), require only gentle (<1°) slopes for their formation (Stow, 1994) and thus could have been generated on the basement topography observed today. However, the rock-fall origin (Gibson et al., this volume) for the serpentinite breccias of Subunit IVA at Site 899 implies the existence of steep slopes nearby (Stow 1994). As this site was only surveyed by *JOIDES Resolution* using low-resolution single-channel seismic survey, its topographic setting is not well constrained.

CHRONOSTRATIGRAPHY

Magnetic polarity and microfossil zonations (calcareous nannofossils, foraminifers, and dinoflagellates) used for Leg 149 sites employed the chronostratigraphical time scales of Harland et al. (1990), Gradstein et al. (1994), and Shackleton et al. (in press).

Magnetostratigraphy

A combined paleomagnetic and biostratigraphic study of the Cenozoic sedimentary sequence was conducted by Zhao et al. (this volume). Continuous and undisturbed Cenozoic sections, of sufficient length to allow the identification of geologically useful magnetic polarity sequences, were obtained from Sites 897, 898, and 900, but not from Sites 899 and 901 (Table 2). Therefore, Sites 899 and 901 were not considered any further by Zhao et al. (this volume).

Sedimentary sections of late Neogene age from Holes 897C, 898A, and 900A recorded a pattern of magnetic polarity reversals that correlates well with the known magnetic polarity time scale for the past 5 Ma, and allows the determination of accurate sediment accumulation rates.

The polarity pattern from the Pliocene-Pleistocene turbidite sequence shows that a reliable magnetostratigraphy can be established from the early Pliocene to the Holocene, including the Gilbert/Gauss boundary (3.58 Ma) through the Matuyama/Brunhes boundary (0.78 Ma). Below the middle Miocene angular unconformity that separates the Pliocene-Pleistocene turbidites from the Miocene and earlier strata, a reliable magnetostratigraphy could not be established because of the extremely weak magnetization of the sediments (Figs. 9-11). This sudden downhole decrease in magnetic signal corresponds in general to a large decrease in iron content and an increase in sulfate concentration (Sawyer, Whitmarsh, Klaus et al., 1994), suggesting magnetic mineral dissolution. This magnetic boundary may be caused by the termination in supply of terrigenous material at the end of the early Miocene and reflects the occurrence of the middle Miocene tectonic folding event.

Biostratigraphy

The biostratigraphic data for Sites 897, 898, 899, and 900 indicate that the stratigraphic column is incomplete between the early Eocene and the late Pleistocene (de Kaenel and Bergen, this volume; Liu, this volume; de Kaenel and Villa, this volume; Liu et al., this volume; Gervais, this volume).

Planktonic Foraminifers

An incomplete foraminiferal biostratigraphy was identified at Sites 897, 898, 899, and 900 (Gervais, this volume) from Upper Cretaceous to Pleistocene sediment. Dissolution and changes in water-mass temperatures affect the quality of biozonation in the Pliocene, Miocene (particularly the latest middle to early late Miocene), and

the early Eocene (Gervais, this volume). Several hiatuses occur throughout the sedimentary column.

Benthic Foraminifers

Benthic foraminifers faunas were investigated from the sediments of Cretaceous to Quaternary age at Sites 897, 898, 899, and 900 (Kuhnt and Collins, this volume; Collins et al, this volume). Knowledge about the abyssal benthic foraminifers in the northeastern Atlantic is limited and sediments were examined to improve biostratigraphic information for sediments deposited below the CCD and to obtain paleoecologic information on the depositional environment of these sites. They provided helpful stratigraphic boundary markers for dating lithologic Unit III (Kuhnt and Collins, this volume).

Calcareous Nannofossils

Calcareous nannofossils are generally common to abundant; preservation is generally good in the upper part of the section. From the upper Aptian to the lower Eocene, major parts of the sediment column are barren of nannofossils, because of deposition below the CCD. A maximum of 38 nannofossils datums (Site 897) could be identified from the Pleistocene to the Lower Cretaceous.

A similar sequence of sedimentation events is seen at Sites 897 to 900, as shown in Figures 12-15, with some differences in the sedimentation rates between sites:

1. From the early Eocene to the middle Miocene, sedimentation rates vary from 4.1 to 12.8 m/m.y., except in the Oligocene/Miocene interval from Site 900, where the sedimentation rate is 17.3 m/m.y.
2. One major middle/late Miocene hiatus, associated with a compressional tectonic event, is found at all sites. The missing time interval is about 2.3 Ma.
3. One lower Pliocene condensed interval, including a short hiatus of about 0.75 Ma, is defined at all sites. At Site 898, the TB 3.1 hiatus (Table 3) and the Pliocene hiatus are grouped together and define a more important hiatus from the middle Miocene to the middle lower Pliocene. The hiatus in Site 898 represents about 7 Ma of missing sediment. Sedimentation rates in the middle Miocene to middle early Pliocene are very low. At Site 897 sedimentation rates vary from 1.7 to 3.8 m/m.y., at Site 898 this period is represented by a hiatus, at Site 899 sediment accumulated at a rate of 1.2 m/m.y., and at Site 900 sedimentation averages 1.3 m/m.y.
4. From the early to the late Pliocene, the sedimentation rates vary from 7.7 m/m.y. (Site 898) to 19.5 m/m.y. (Site 900).
5. One condensed interval, or hiatus, restricted to the uppermost Pliocene, is determined at Sites 898, 899, and 900. No hiatus occurred in this interval at Site 897.
6. A relatively thick Pleistocene interval with very high sedimentation rates occurs at all sites from 32.8 m/m.y (Site 900) to 90 m/m.y. (Site 898).

Figure 16 presents the accumulation rates for Cenozoic sediments at Sites 897, 898, and 900 in further detail. The average accumulation rate over the whole Pliocene-Pleistocene turbidite sequence varies between the three sites, increasing with increasing water depth. The rate averages 99 m/m.y. at Site 897 (Fig. 16A). The overall average is 92 m/m.y. at Site 898, but single rates vary from 64.8 m/m.y. (1.95-1.46 Ma) to a rapid 167 m/m.y. (1.46-1 Ma) and then back to 71 m/m.y. (1 Ma to the present) (Fig. 16B). This interval of higher accumulation rate corresponds in part to thicker and more sandy turbidites, which occur in Cores 149-898-8H to 10H. The sedimentation rate at Site 900 (25.8 m/m.y.) is fairly constant through the Pleistocene (Fig. 16C) and declines to 10.6 m/m.y. for the late Pliocene. This change is consistent with accumulation within the lysocline but
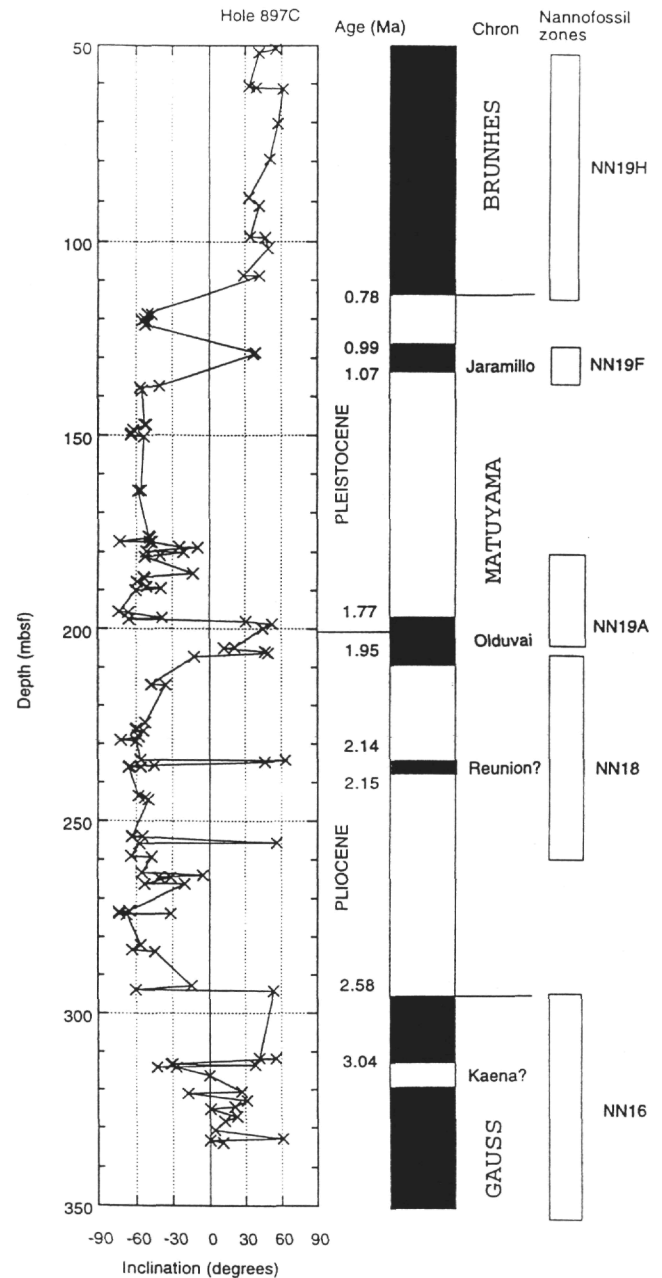
Figure 9. Downhole variations of stable magnetic inclination, inferred polarity, and biostratigraphic zones for Cenozoic sediments from Hole 897C (from Zhao et al., this volume). Normal polarity is represented by black areas; reversed polarity is represented by white areas.

above the CCD, where a proportion of the $CaCO_3$ deposited on the seabed is dissolved before burial. In Site 897, the pelagic clay sequence immediately beneath the Pliocene/Pleistocene turbidites has an accumulation rate of 4.2 m/m.y. (Milkert et al., this volume). This is consistent with an elevated CCD prior to the onset of Northern Hemisphere glaciation at 2.6 Ma.

DEPOSITIONAL HISTORY ON THE IBERIA ABYSSAL PLAIN

The depositional history of the Iberia Abyssal Plain is generally characterized through its history by the influence of downslope trans-
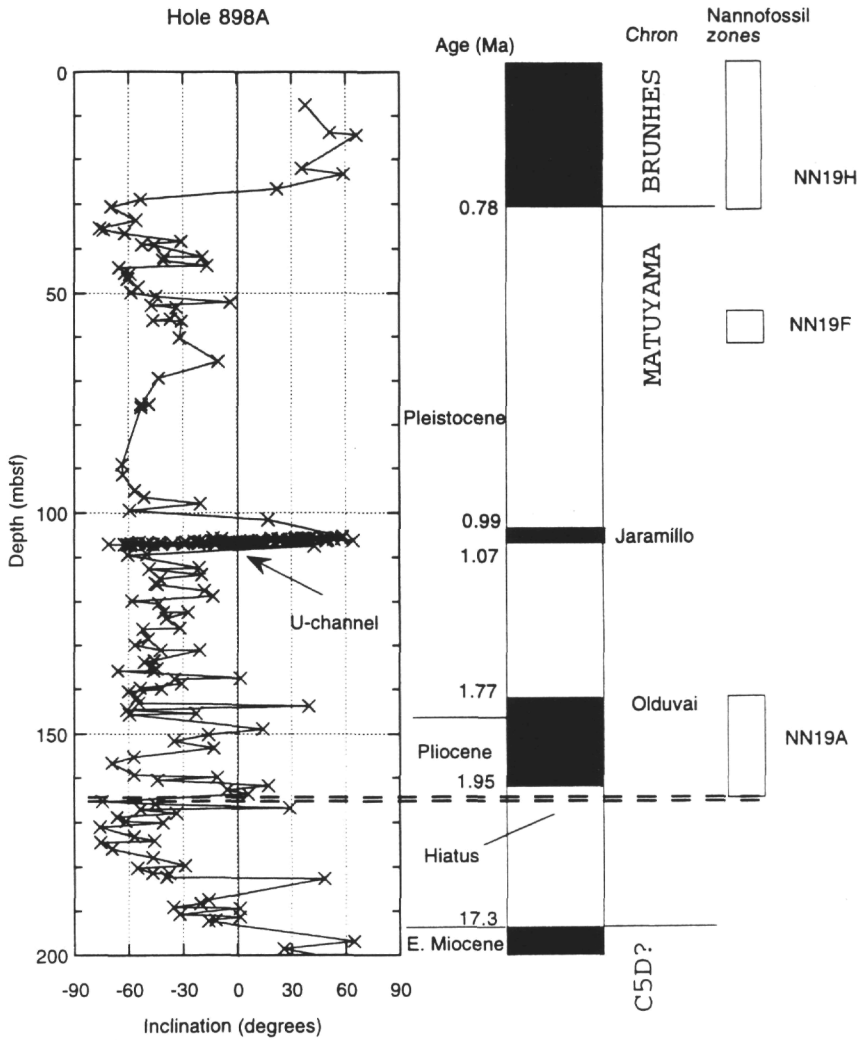
Figure 10. Downhole variations of stable magnetic inclination, inferred polarity, and biostratigraphic zones for Cenozoic sediments at Hole 898A (from Zhao et al., this volume). Normal polarity is represented by black areas; reversed polarity is represented by white areas.

port of terrigenous sediments. Various types of debris-flow deposits, turbidity-current deposits, and contour-current reworking can be found. This may have been favored by low sea levels and by catastrophic events such as slope failure, triggered, for example, by earthquakes or oversteepening (Middleton and Hampton, 1976). Two sources for the sediments could be verified: (1) the input of material form the continental margin, which can be shown by the terrigenous composition of the turbidites, and (2) the input from local morphological highs, expressed by the high abundance of foraminifers. The major role of sedimentation is displayed by the narrow continental shelf incised by submarine canyons.

The sedimentology, biostratigraphy, magnetostratigraphy, and seismostratigraphy of the Iberia Abyssal Plain area suggest the following five stages for the evolution of the abyssal plain. These stages are the major features of an integrated depositional model (Fig. 17).

Stage 1. Upper Cretaceous and Lower Tertiary Gravitational Flows

The last stages of rifting probably occurred between 140 and 135 Ma (Wilson et al., this volume). No evidence could be found to suggest that the basement topography established during rifting was modified by postrift deformation. For example, there is no evidence that the basement ridge at Site 897 was tectonically uplifted or rose diapirically later (however, see Whitmarsh and Sawyer, this volume). Older Cretaceous sediments (early Aptian age) consist of heterogeneous discrete sediment bodies mixed or intercalated with mafic and ultramafic rocks. Sediments in Unit IV yield an early Aptian age. The oldest sedimentary equivalent to seismostratigraphic unit 6 is of Aptian to possibly Valanginian age (Wilson et al., this volume), which increases the difficulty of interpreting the setting of the Aptian debris flows and rock-fall breccias encountered on the crest of basement highs at Sites 897 and 899.

Stage 2. Eocene Pelagic Sedimentation

The Eocene red clays of lithologic Subunit IIIA are interpreted as probably the product of slow accumulation of clay in an oxygenated environment, possibly below the CCD (Shipboard Scientific Party, 1994a, c, d), which agrees well with the results of other DSDP/ODP drilling programs along the northeastern Atlantic continental margin (Sibuet and Ryan, 1979; Boillot, Winterer, Meyer, et al., 1987). During the Eocene-Paleocene, the regional CCD was relatively shallow (Emery and Uchupi, 1984). At the Site 900, the most landward site, the Eocene is dominated by deposition and reworking by contour currents.

Stage 3. Oligocene and Miocene Contourites

Sites 897, 898, and 900 all contain middle Miocene contourite sequences interbedded with pelagic clays. Parts of the middle Miocene to upper Pliocene are missing from Sites 897 and 898 because of a hiatus associated with crustal compression and sediment folding during the middle Miocene (Masson et al., 1994; Sawyer, Whitmarsh, Klaus, et al., 1994). The sediment sequence is more
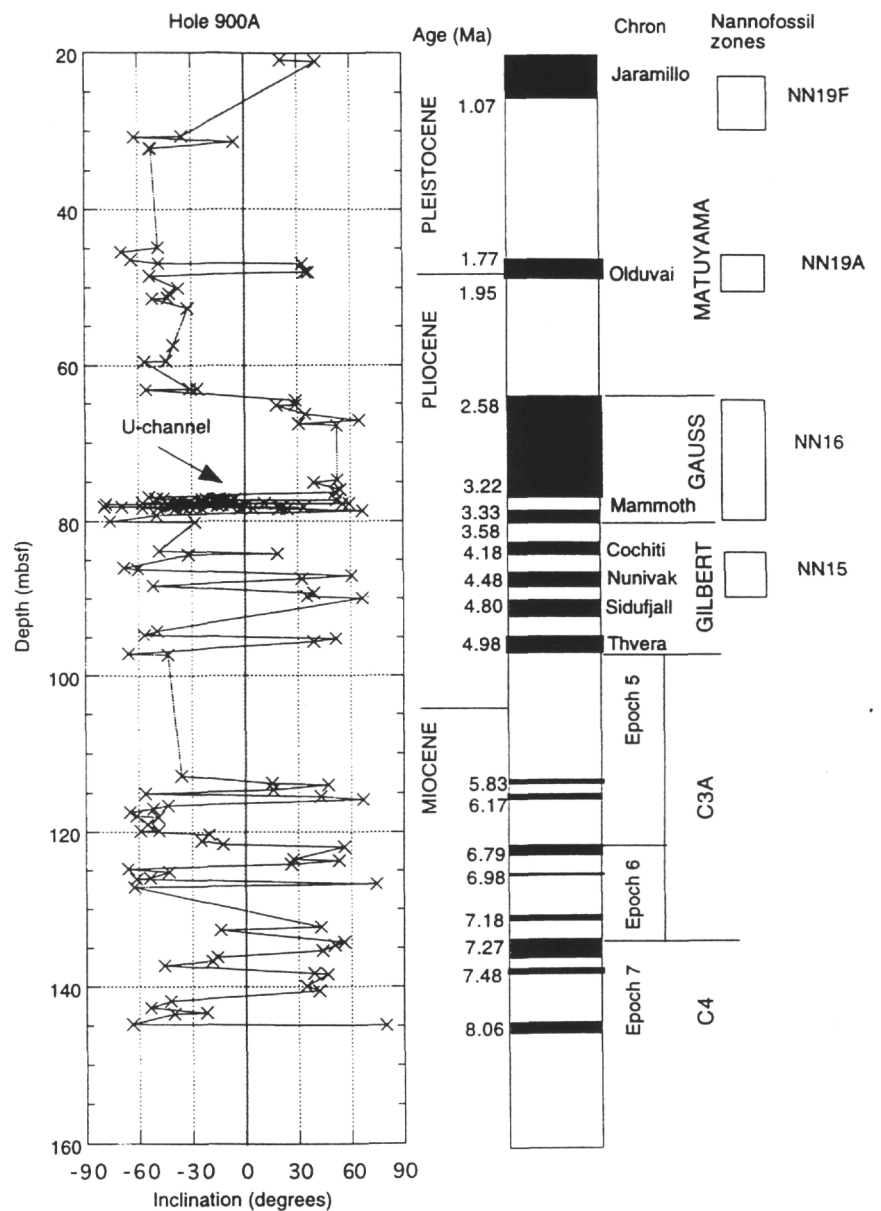
Figure 11. Downhole variations of stable magnetic inclination, inferred polarity, and biostratigraphic zones for Cenozoic sediments at Hole 900A (from Zhao et al., this volume). Normal polarity is represented by black areas; reversed polarity is represented by white areas.

complete at Site 900 where the middle Miocene contourites pass upwards into a sequence of thin mud turbidites interbedded with pelagic sediments at around 15.8 Ma (Fig. 17). The number of turbidites gradually decreases upwards in the upper Miocene (around 9.9 to 8.2 Ma; Gervais, this volume) from Cores 149-900A-15R (124 mbsf) to 12R (98 mbsf). Between 8.4 and 5.56 Ma, turbidites disappear completely, giving way to a continuous sequence of pelagic marls.

Stage 4. Miocene Compressional Phase

The upper Miocene hiatus at Site 897, 898, and 899 occurs at the top of the contourite sequence and represents a sediment gap of 2.3 Ma (Fig. 17). Above the hiatus are a few meters of pelagic clays, succeeded by the Pliocene-Pleistocene turbidite sequence.

Stage 5. Pliocene and Pleistocene Turbidite Sedimentation

Pliocene and Pleistocene turbidites on the Iberia Abyssal Plain represent a distinct change in sediment type from the contourites, mud turbidites, and pelagic sediments beneath.

The major input of deposits from terrigenous turbidites into the Iberia Abyssal Plain starts in the late Pliocene at 2.6 Ma and follows a period of pelagic deposition that lasted at least a few million years at Sites 897 and 900. The frequency of turbidity currents varies from 20.5 flows/100 k.y. between 1.8 and 2 Ma to 64 flows/100 k.y. between 1.2 to 1.4 Ma, and reduce gradually to the present day (Milkert et al, this volume). At the eastern Site 900, the highest rate includes 8 flows/100 k.y. between 1.6 and 2 Ma. The mechanism for initiating flows appears to be earthquakes, although the onset of Pliocene/Pleistocene turbidite deposition may have been influenced by the onset of Northern Hemisphere glaciation. The coincidence of the 2.6 Ma age of onset of turbidite deposition with the onset of Northern Hemisphere glaciation (Shackleton et al., 1984) is striking. Weaver and Kuijpers (1983) showed a link between climate/sea level change and turbidite deposition on the Madeira Abyssal Plain, and Weaver et al. (1986) postulated that the Madeira Abyssal Plain would receive turbidites during periods of climatic oscillation such as the 2.6 Ma to Holocene interval. The onset of turbidite deposition at 2.6 Ma suggests that sedimentation in the Iberian Basin is at least partially controlled by climatic change. However, the frequency of turbidite input is much greater than in
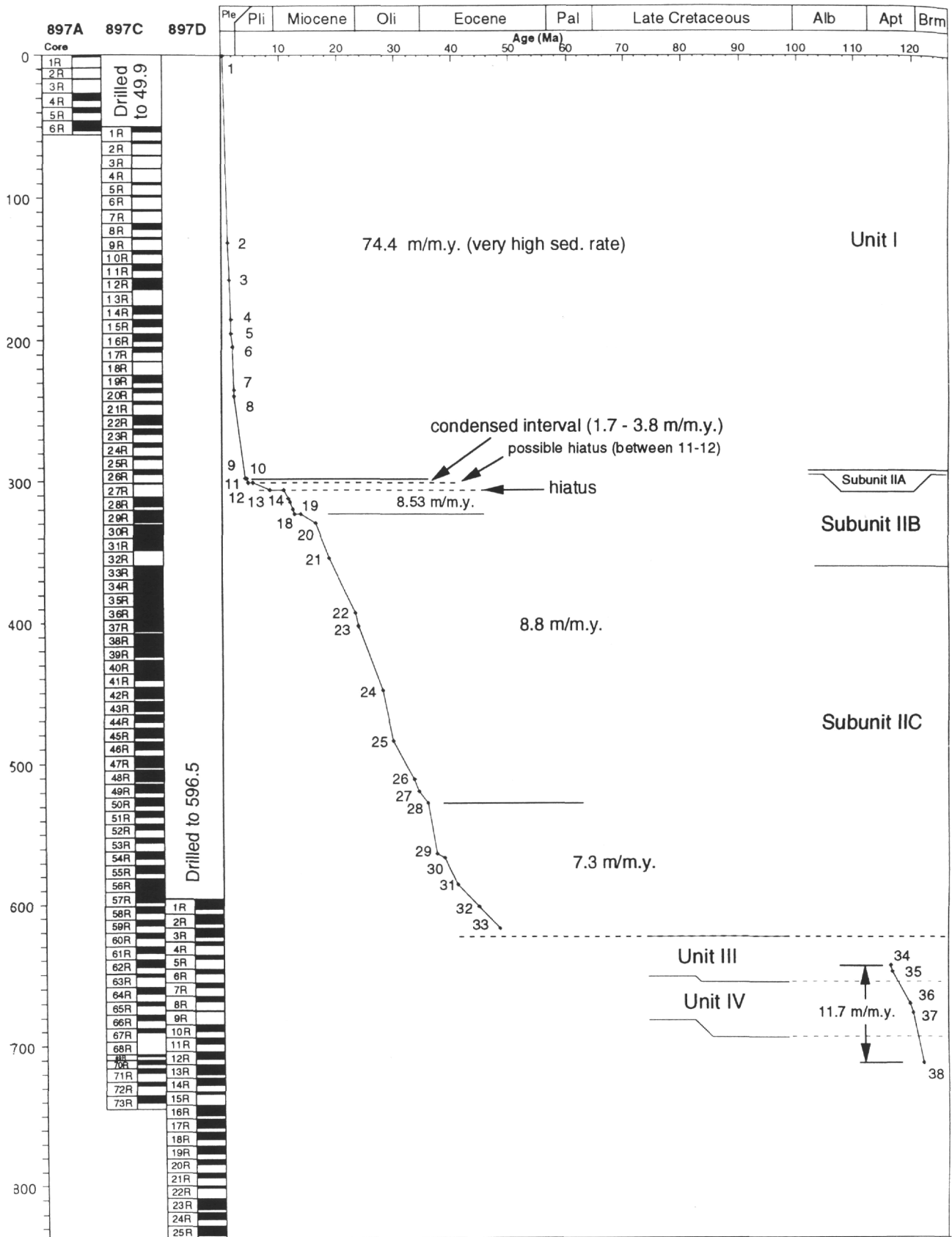
Figure 12. Age vs. depth plots for Site 897 with core recovery. Data are based on the nannofossil datums given in Table 3.
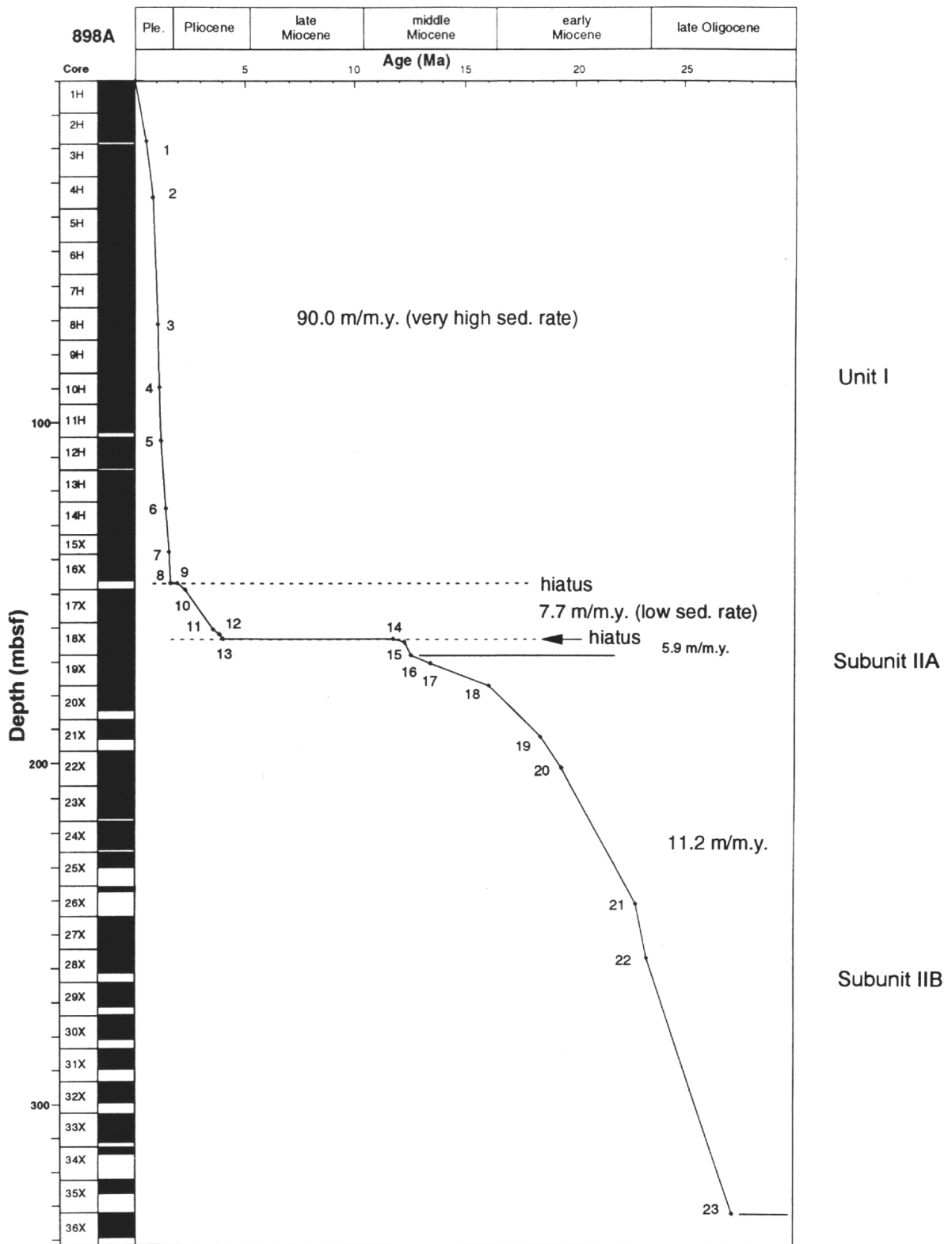
Figure 13. Age vs. depth plots for Site 898 with core recovery. Data are based on the nannofossil datums given in Table 3.
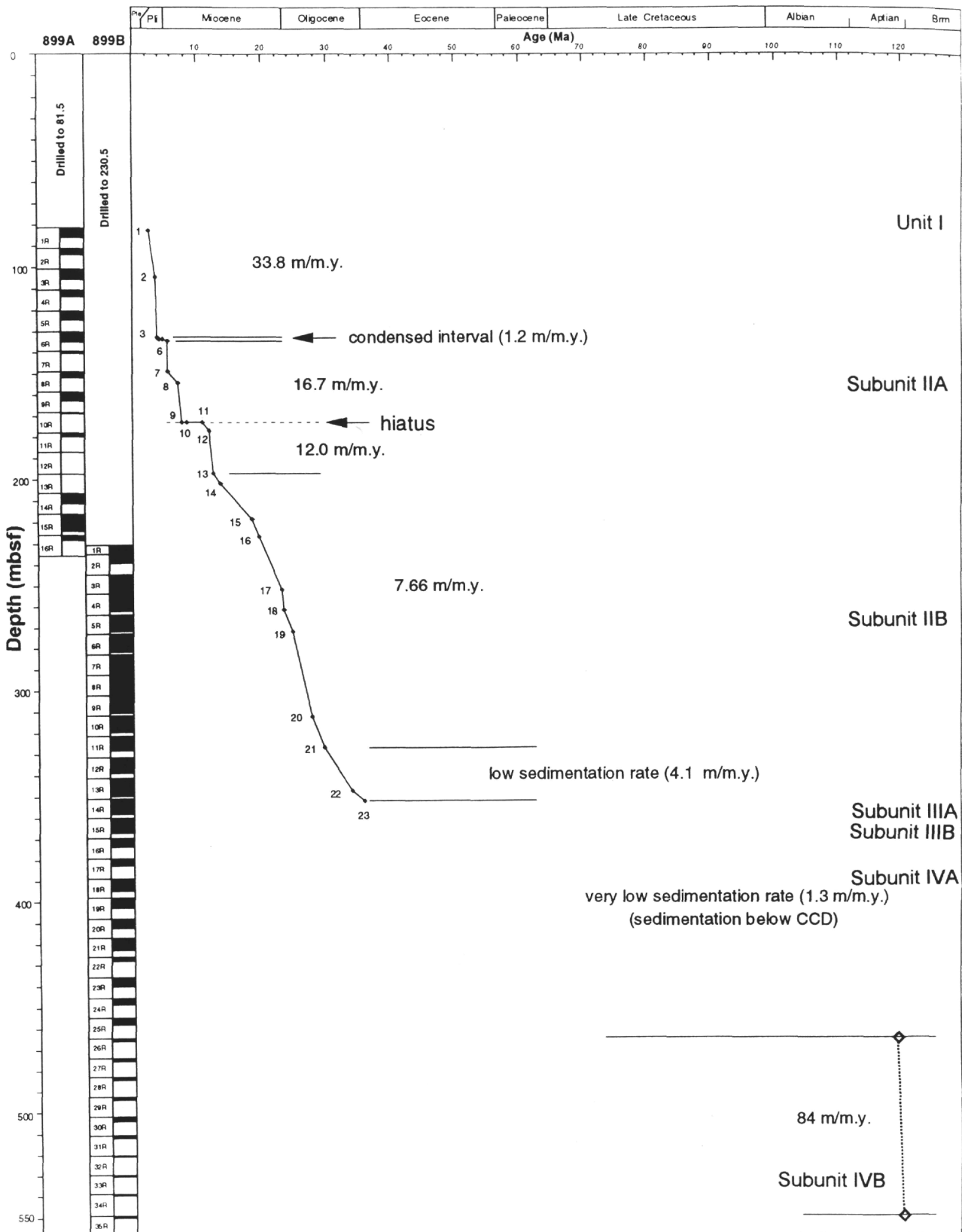
Figure 14. Age vs. depth plots for Site 899 with core recovery. Data are based on the nannofossil datums given in Table 3.
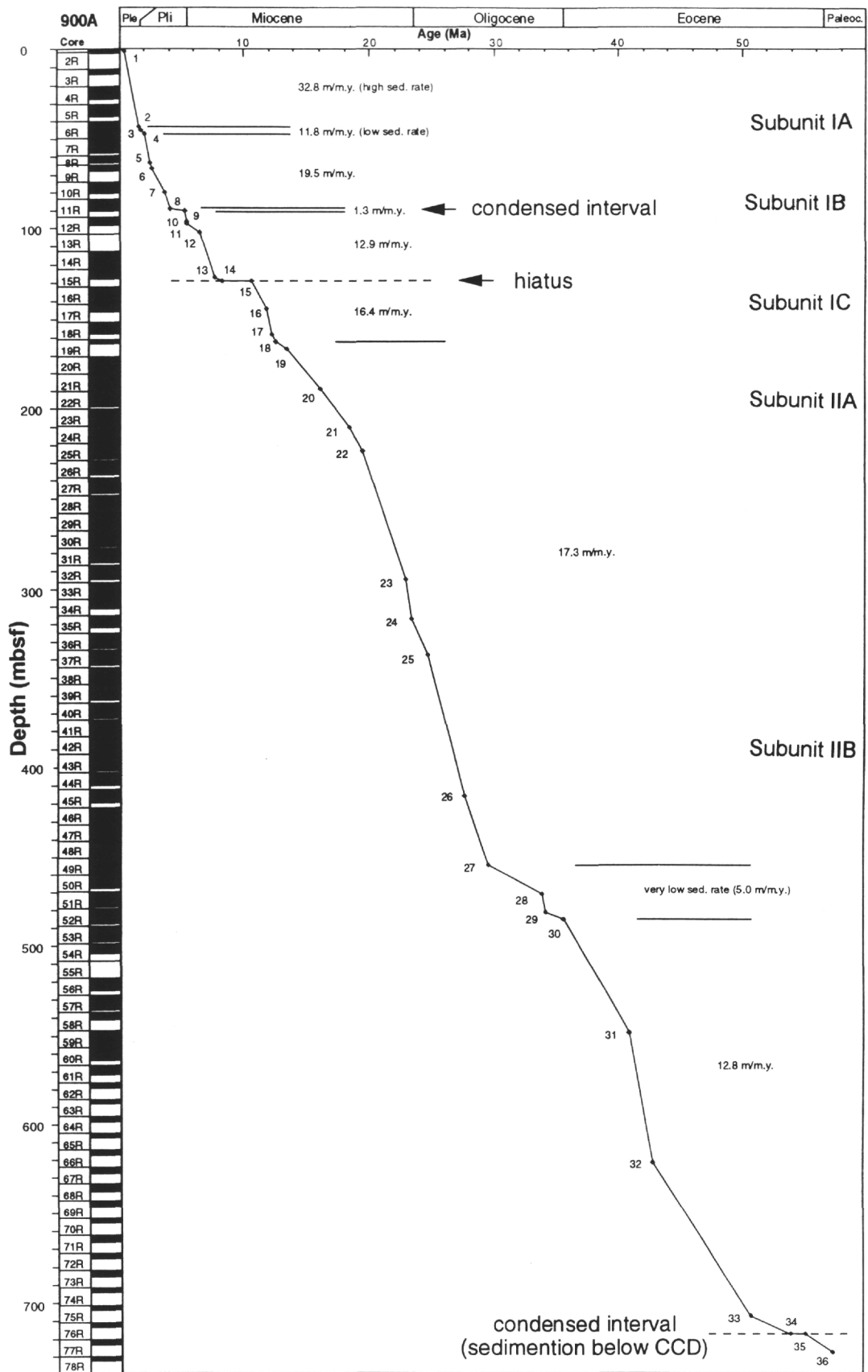
Figure 15. Age vs. depth plots for Site 900 with core recovery. Data are based on the nannofossil datums given in Table 3.

Table 3. Stratigraphic placement in meters (to nearest decimeter) of the Site 897 to Site 900 chron and subchron boundaries.

Age (Ma)	Zonation	Site 897		Site 898		Site 899		Site 900	
		Depth range (mbsf)	Depth boundary (mbsf)	Depth range (mbsf)	Depth boundary (mbsf)	Depth range (mbsf)	Depth boundary (mbsf)	Depth range (mbsf)	Depth boundary (mbsf)
0.26	B *E. huxleyi*		1.32						1.87
0.46	T *P. lacunosa*			17.82	17.76–17.89				
0.81	T *Reticulofenestra* sp. A (>6.5)			34.51	31.32–37.70				
0.98	B *Reticulofenestra* sp. A (>6.5)			71.34	66.98–75.70				
1.10	T *Gephyrocapsa* spp. (>5.5)			90.00	85.2–94.7				
1.12	T *H. sellii*	123.31–139.59	131.45						
1.19	T common *H. sellii*			105.60					
1.37	B *Gephyrocapsa* spp. (>5.5)			125.35	123.60–127.11				
1.54	T *C. macinteyri* (>11.)	151.13–165.1	158.11	138.25	137.32–139.19				43.92
1.58	B *G. oceanica* (>4.0)		186.19						
1.64	B *G. caribbeanica* (>4.)		195.47						45.95
1.88	T *D. brouweri*	200.32–208.95	204.63	147.4	146.19–148.62				47.92
2.12	BA *D. triradiatus*	235.13–235.72	235.42						
2.27	T *D. pentaradiatus*	236.82–243.43	240.12	149.00	148.62–149.38				
2.40	T *D. surculus*					83.44–83.19	83.31	64.43	
2.60	T *D. tamalis*								66.82
3.45	T *S. abies/R. pseudoumbilicus*					105.45–104.89	105.19		
3.56	T *R. pseudoumbilica*			161.16	160.53–161.80	80.08			
3.86	T *S. abies*			162.44	161.68–163.2				
3.87	B Acme *D. asymmetricus*					133.52–132.57	133.04		
4.0	B *P. lacunosa*	294.08–301.21	297.64	163.67		133.52–134.45	133.98	89.39–89.12	89.25
4.3	T *A. delicatus*	294.08–301.21	297.64						
4.43	B *C. christatus*	301.25–301.72	301.48			133.52–134.45	133.98		
5.17	T *A. delicatus*–T *A. primus*							90.15–89.39	90.77
5.30	T *T. rugosus*	301.25–301.72	301.48				134.71		96.98
5.38	T *D. quinqueramus*						149.23		98.15
6.34	B *A. amplificus*								103.07
7.01	B *A. primus*						155.00		
7.60	B *D. quinqeramus*						173.22		127.46
8.20	Top TB3.1		306.45				173.22		129.81
10.5	Base TB3.1		306.45				173.22		129.81
11.50	T *D. kugleri*		312.38						
11.70	T *C. floridanus* (cons. occ.)		315.19	163.70	144.33				
12.20	B *D. kugleri*		319.78	164.76			179.39		159.25
12.50	B *T. rugosus*		323.51	168.36			197.16		162.64
13.37	T *S. heteromorphus*		323.51	170.76			202.20		167.08
16.00	T *H. ampliaperta*		329.91	177.46			189.65		
18.42	B *S. heteromorphus*		353.82	192.54			219.20		210.79
19.40	B *S. belemnos*			201.77			227.38		224.33
22.80	B *D. druggli*		392.85	241.72			252.01		295.31
23.30	T *R. bisecta*		403.23	257.73			261.81		317.28
24.60	T LCO *S. ciperoensis*						272.71		338.26
27.60	T *S. distentus*		448.01	333.27			312.46		416.90
29.40	B *S. ciperoensis*		483.76				326.69		455.01
33.10	B *S. distentus*		511.19						
33.70	T *R. umbilica*						347.28		471.07
34.00	T *E. formosa*		518.8						481.50
35.60	T *D. saipanensis*	526.92–527.48	527.2			352.30			485.59
37.10	B *I. recurvus*	562.75–564.66	563.71						
38.40	B *C. oamaruensis*	562.75–571.88	567.31						
40.80	T *C. solitus*	581.91–589.48	585.69				548.82		
42.80	T *Nannotetrina* spp.								622.35
44.40	T *B. gladius*	598.02–606.14	602.08						
48.10	B *N. alata*	613.25–622.97	618.11						
50.80	B *D. sublodoensis*							703.78–710.57	707.18
54.00	B *D. lodoensis*							722.7–713.29	717.72
55.20	T *T. contortus*							722.7–713.29	717.72
57.50	B *D. multiradiatus*								727.81
116.40	B *P. spinosa*	644.01–648.71	644.01						
116.60	T *C. rothii/M. hochulzii*		648.64						
119.80	B *R. angustus*		670.72				465.01		
120.50	B *H. irrularis*		677.40				549.38		
122.30	B *R. achlyostaurion/F. oblongus* (early)		712.80						

Note: * after Shipboard Scientific Party, (1994a); de Kaenel and Bergen, (this volume); Kuhnt and Collins, (this volume); Zhao et al., (this volume). B = bottom, T = top, LCO = last common occurrence.

the Madeira Abyssal Plain and individual turbidites are clearly not related to particular sea-level changes, as they are for the Madeira Abyssal Plain. It may be that the lowering of sea level, associated with the buildup of Northern Hemisphere ice, caused a narrowing of the continental shelves, and thus allowed more sediment to be dumped beyond the shelf edge, in turn causing the margins to become unstable. Higher rates of accumulation on the upper parts of the slope may have led to unstable sediment accumulation, which could have resulted in earthquake-triggered sediment removal by turbidity flows.

A short sedimentary hiatus in the early Pleistocene, or at least a decrease in accumulation rate, was recognized at three sites (Sites 897, 898, and 900; Zhao et al., this volume). This hiatus may represent an oceanographic event that affected a significant part of the Iberia Abyssal Plain region and may also be correlated to the onset of Northern Hemisphere glaciation (Milkert et al., this volume).

REFERENCES

Abate, E., Bortolotti, V., and Passerini, P., 1970. Olistostromes and olitholiths. *In* Sestini, E. (Ed.), Development of the Northern Apennines Geosincline. *Sediment. Geol.,* 4:521-537.

Bernoulli, D., and Weissert, H., 1985. Sedimentary fabrics in Alpine ophicalcites, South Pennine Arosa Zone, Switzerland. *Geology,* 13:755-758.

Beslier, M.O., Ask, M., and Boillot, G., 1993. Ocean-continent boundary in the Iberia Abyssal Plain from multichannel seismic data. *Tectonophysics,* 218:383-393.

Boillot, G., Auxiètre, J.L., Dunand, J.P., Dupeuble, P.A., and Mauffret, A., 1979. The northwestern Iberian margin: a Cretaceous passive margin deformed during Eocene. *In* Talwani, M., Hay, W., and Ryan, W.B.F. (Eds.), *Deep Drilling Results in the Atlantic Ocean: Continental Margin and Paleoenvironment.* Am. Geophys. Union, Maurice Ewing Ser., 3:138-153.

Boillot, G., Comas, M.C., Girardeau, J., Kornprobst, J., Loreau, J.-P., Malod, J., Mougenot, D., and Moullade, M., 1988. Preliminary results of the Galinaute cruise: dives of the submersible *Nautile* on the Western Galicia Margin, Spain. *In* Boillot, G., Winterer, E.L., et al., *Proc. ODP, Sci. Results,* 103: College Station, TX (Ocean Drilling Program), 37-51.

Boillot, G., Grimaud, S., Mauffret, A., Mougenot, D., Kornprobst, J., Mergoil-Daniel, J., and Torrent, G., 1980. Ocean-continent boundary off the Iberian margin: a serpentinite diapir west of the Galicia Bank. *Earth Planet. Sci. Lett.,* 48:23-34.

Boillot, G., Winterer, E.L., Meyer, A.W., et al., 1987. *Proc. ODP, Init. Repts.,* 103: College Station, TX (Ocean Drilling Program).

Bonatti, E., Emiliani, C., Ferrara, G., Honnorez, J., and Rydell, H., 1974. Ultramafic-carbonate breccias from the equatorial Mid Atlantic Ridge. *Mar. Geol.,* 16:83-102.

Bonatti, E., Honnorez, J., and Gartner, S., Jr., 1973. Sedimentary serpentinites from the Mid-Atlantic Ridge. *J. Sediment. Petrol.,* 43:728-735.

Bouma, A.H., 1962. *Sedimentology of Some Flysch Deposits: A Graphic Approach to Facies Interpretation:* Amsterdam (Elsevier).

Comas, M.C., and Maldonado, A., 1988. Late Cenozoic sedimentary facies and processes in the Iberian Abyssal Plain, Site 637, ODP Leg 103. *In* Boillot, G., Winterer, E.L., et al., *Proc. ODP, Sci. Results,* 103: College Station, TX (Ocean Drilling Program), 635-655.

Davies, T.A., 1967. Recent sedimentation in the Northeast Atlantic [Ph.D. dissert.]. Univ. Cambridge, U.K.

de Lange, G.J., Jarvis, I., and Kuijpers, A., 1987. Geochemical characteristics and provenance of late Quaternary sediments from the Madeira Abyssal Plain, North Atlantic. *In* Weaver, P.P.E., and Thomson, J. (Eds.), *Geology and Geochemistry of Abyssal Plains.* Geol. Soc. Spec. Publ. London, 31:147-165.

Einsele, G., 1992. *Sedimentary Basins:* Berlin (Springer-Verlag).

Emery, K.O., and Uchupi, E., 1984. *The Geology of the Atlantic Ocean:* New York (Springer-Verlag).

Faugères, J.C., Gonthier, E., and Stow, D.A.V., 1984. Contourite drift moulded by deep Mediterranean outflow. *Geology,* 12:296-300.

Faugères, J.C., and Stow, A.V., 1993. Bottom-current-controlled sedimentation: a synthesis of the contourite problem. *Sediment. Geol.,* 82:287-297.

Fonseca, J.F.B.D., and Long, R.E., 1989. Seismotectonics of Western Portugal. *Proc. 4th Symp. Analysis of Seismicity and Seismic Risk,* Bechyne Castle, Czechoslovakia, 266-273.

Gardner, J.V., and Kidd, R.B., 1987. Sedimentary processes on the northwestern Iberian continental margin viewed by long-range side-scan sonar and seismic data. *J. Sediment. Petrol.,* 57:397-407.

Gradstein, F.M., Agterberg, F.P., Ogg, J.G., Hardenbol, J., van Veen, P., Thierry, J., and Huang, Z., 1994. A Mesozoic time scale. *J. Geophys. Res.,* 99:24051-24074.

Grimsison, N.I., and Chen, W.-P., 1986. The Azore-Gibraltar plate boundary: focal mechanism, depths of earthquakes and their tectonic implications. *J. Geophys. Res.,* 91:2029-2047.

Groupe Galice, 1979. The continental margin off Galicia and Portugal: acoustical stratigraphy, dredge stratigraphy, and structural evolution. *In* Sibuet, J.-C., Ryan, W.B.F., et al., *Init. Repts. DSDP,* 47 (Pt. 2): Washington (U.S. Govt. Printing Office), 633-662.

Hallam, A., 1971. Facies analysis of the Lias of West Central, Portugal. *Neues. Jahrb. Geol. Palaeontol.,* 139:226-265.

Harland, W.B., Armstrong, R.L., Cox, A.V., Craig, L.E., Smith, A.G., and Smith, D.G., 1990. *A Geologic Time Scale 1989:* Cambridge (Cambridge Univ. Press).

Kidd, R.B., 1982. Long-range sidescan sonar studies of sediment slides and the effects of slope mass sediment movement on abyssal plain sedimentation. *In* Saxov, S., and Nieuwenhuis, J.K. (Eds.), *Marine Slides and Other Mass Movements:* New York (Plenum Press), 289-303.

Kidd, R.B., and Roberts, D.G., 1982. Long-range sidescan sonar studies of large-scale features in the North Atlantic. *Bull. Inst. Geol. Bassin Aquitaine,* 31:11-29.

Laughton, A.S., Roberts, D.G., and Graves, R., 1975. Bathymetry of the Northeast Atlantic: Mid-Atlantic Ridge to Southwest Europe. *Deep-Sea Res.,* 22:791-810.

Martins, I., and Victor, L.A.M, 1990. *Contribuicao para o estudo da sismicidade de Portugal continental.* Univ, de Lisboa, Inst. Geofisico do Infante d. Luis, Publ. 18.

Masson, D.G., Cartwright, J.A., Pinheiro, L.M., Whitmarsh, R.B., Beslier, M.-O., and Roeser, H., 1994. Compressional deformation at the ocean-continent transition in the NE Atlantic. *J. Geol. Soc. London,* 151:607-613.

Middleton, G.V., and Hampton, M.A., 1976. Subaqueous sediment transport and deposition by gravity flows. *In* Stanley, D.J., and Swift, D.J.P. (Eds.), *Marine Sediment Transport and Environmental Management:* New York (J. Wiley and Sons), 197-218.

Moreira, V.S., 1985. Seismotectonics of Portugal and its adjacent area in the Atlantic. *Tectonophysics,* 117:85-96.

Mougenot, D., 1988. Géologie de la Marge Portugaise [thése de Doctorat d'Etat des Sciences Naturelles]. Univ. Pierre et Marie Curie, Paris.

Mougenot, D., Kidd, R.B., Mauffret, A., Regnauld, H., Rothwell, G., and Vanney, J.-R., 1984. Geological interpretation of combined seabeam, Gloria and seismic data from Porto and Vigo seamounts, Iberian Continental Margin. *Mar. Geophys. Res.,* 6:329-363.

Mougenot, D., Vanney, J.R., Mauffret, A., and Kidd, R.B., 1985. Les montagnes sous-marins de la marge continentale nord-porugaise: morphologie et evolution structurale. *Bull. Soc. Geol. Fr.,* 9:401-412.

Raymo, M.E., Ruddiman, W.F., and Clement, B.M., 1987. Pliocene-Pleistocene paleoceanography of the North Atlantic at DSDP Site 609. *In* Ruddiman, W.F., Kidd, R.B., Thomas, E., et al., *Init. Repts. DSDP,* 94 (Pt. 2): Washington (U.S. Govt. Printing Office), 895-901.

Ribeiro, A., Antunes, M.T., Ferreira, M.P., Rocha, R.B., Soares, A.F., Zbyszewski, G., Moitinho de Almeida, F., Carbalho, D., and Monteiro, J.H., 1979. *Introduction à la Gèologie Generale du Portugal:* Lisboa (Ed Serv. Geol. de Portugal).

Roberts, D.G., and Kidd, R.B., 1984. Sedimentary and structural patterns on the Iberian continental margin: an alternative view of continental margin sedimentation. *Mar. Pet. Geol.,* 1:37-48.

Ryan, W.B.F., Hsü, K.J., et al., 1973. *Init. Repts. DSDP,* 13 (Pts. 1 and 2): Washington (U.S. Govt. Printing Office).

Sawyer, D.S., Whitmarsh, R.B., Klaus, A., et al., 1994. *Proc. ODP, Init. Repts.,* 149: College Station, TX (Ocean Drilling Program).

Shackleton, N.J., Backman, J., Zimmerman, H., Kent, D.V., Hall, M.A., Roberts, D.G., Schnitker, D., Baldauf, J.G., Desprairies, A., Homrighausen, R., Huddlestun, P., Keene, J.B., Kaltenback, A.J., Krumsiek, K.A.O., Morton, A.C., Murray, J.W., and Westberg-Smith, J., 1984. Oxygen isotope calibration of the onset of ice-rafting and history of glaciation in the North Atlantic region. *Nature,* 307:620-623.

Shackleton, N.J., Crowhurst, S., Hagelberg, T., Pisias, N.G., and Schneider, D.A., 1995. A new late Neogene time scale: application to Leg 138 sites. *In* Pisias, N.G., Mayer, L.A., Janecek, T.R., Palmer-Julson, A., and van Andel, T.H. (Eds.), *Proc. ODP, Sci. Results,* 138: College Station, TX (Ocean Drilling Program), 73-101.

Shipboard Scientific Party, 1979. Site 398. *In* Sibuet, J.-C., Ryan, W.B.F., et al., *Init. Repts. DSDP,* 47 (Pt. 2): Washington (U.S. Govt. Printing Office), 25-233.

Shipboard Scientific Party, 1994a. Site 897. *In* Sawyer, D.S., Whitmarsh, R.B., Klaus, A., et al., *Proc. ODP, Init. Repts.,* 149: College Station, TX (Ocean Drilling Program), 41-113.

———, 1994b. Site 898. *In* Sawyer, D.S., Whitmarsh, R.B., Klaus, A., et al., *Proc. ODP, Init. Repts.,* 149: College Station, TX (Ocean Drilling Program), 115-146.

———, 1994c. Site 899. *In* Sawyer, D.S., Whitmarsh, R.B., Klaus, A., et al., *Proc. ODP, Init. Repts.,* 149: College Station, TX (Ocean Drilling Program), 147-209.

———, 1994d. Site 900. *In* Sawyer, D.S., Whitmarsh, R.B., Klaus, A., et al., *Proc. ODP, Init. Repts.,* 149: College Station, TX (Ocean Drilling Program), 211-262.

———, 1994e. Site 901. *In* Sawyer, D.S., Whitmarsh, R.B., Klaus, A., et al., *Proc. ODP, Init. Repts.,* 149: College Station, TX (Ocean Drilling Program), 263-268.

Sibuet, J.-C., and Ryan, W.B.F., 1979. Site 398: evolution of the west Iberian passive continental margin in the framework of the early evolution of the North Atlantic Ocean. *In* Sibuet, J.-C., Ryan, W.B.F., et al., *Init. Repts. DSDP,* 47 (Pt. 2): Washington (U.S. Govt. Printing Office), 761-775.

Siebert, L., 1984. Large volcanic debris avalanches: characteristics of source areas, deposits and associated eruptions. *J. Volcanol. Geotherm. Res.,* 22:163-197.

Stoopes, G.R., and Sheridan, M.F., 1992. Giant debris avalanches from the Colima volcanic complex, Mexico: implications for long-runout landslides (>100 km) and hazard assessment. *Geology,* 20:129-132.

Stow, D.A.V., 1994. Deep sea processes of sediment transport and deposition. *In* Pye, K. (Ed.), *Sediment Transport and Depositional Processes:* London (Blackwell), 257-291.

Stow, D.A.V., and Piper, D.J.W., 1984. Deep-water fine-grained sediments: history, methodology, and terminology. *In* Stow, D.A.V., and Piper, D.J.W. (Eds.), *Fine-Grained Sediments: Deep-Water Processes and Facies.* Geol. Soc. Spec. Publ. London, 15:3-14.

Watson, R.A., and Wright, H.E., Jr., 1969. The Saidmarreh landslide, Iran. In *U.S. Contributions to Quaternary Research.* Spec. Pap.—Geol. Soc. Am., 123:115-139.

Weaver, P.P.E., and Kuijpers, A., 1983. Climatic control of turbidite deposition on the Madeira Abyssal Plain. *Nature,* 306:360-363.

Weaver, P.P.E., Searle, R.C., and Kuijpers, A., 1986. Turbidite deposition and the origin of the Madeira Abyssal Plain. *In* Summerhayes, C.P., and Shackleton, N.J. (Eds.), *North Atlantic Palaeoceanography.* Spec. Publ. Geol. Soc. London, 21:131-143.

Whitmarsh, R.B., Miles, P.R., and Mauffret, A., 1990. The ocean-continent boundary off the western continental margin of Iberia, I. Crustal structure at 40°30'N. *Geophys. J. Int.,* 103:509-531.

Whitmarsh, R.B., Pinheiro, L.M., Miles, P.R., Recq, M., and Sibuet, J.C., 1993. Thin crust at the western Iberia ocean-continent transition and ophiolites. *Tectonics,* 12:1230-1239.

Wilson, R.C.L., Hiscott, R.N., Willis, M.G., and Gradstein, F.M., 1989. The Lusitanian Basin of west-central Portugal: Mesozoic and Tertiary tectonic, stratigraphic and subsidence history. *In* Tankard, A.J., and Balkwill, H.R. (Eds.), *Extensional Tectonics and Stratigraphy of the North Atlantic Margins.* AAPG Mem., 46:341-361.

Yarnold, J.C., 1993. Rock-avalanche characteristics in dry climates and the effect of flow into lakes: insights from mid-Tertiary sedimentary breccias near Artillery Peak, Arizona. *Geol. Soc. Am. Bull.,* 105:345-360.
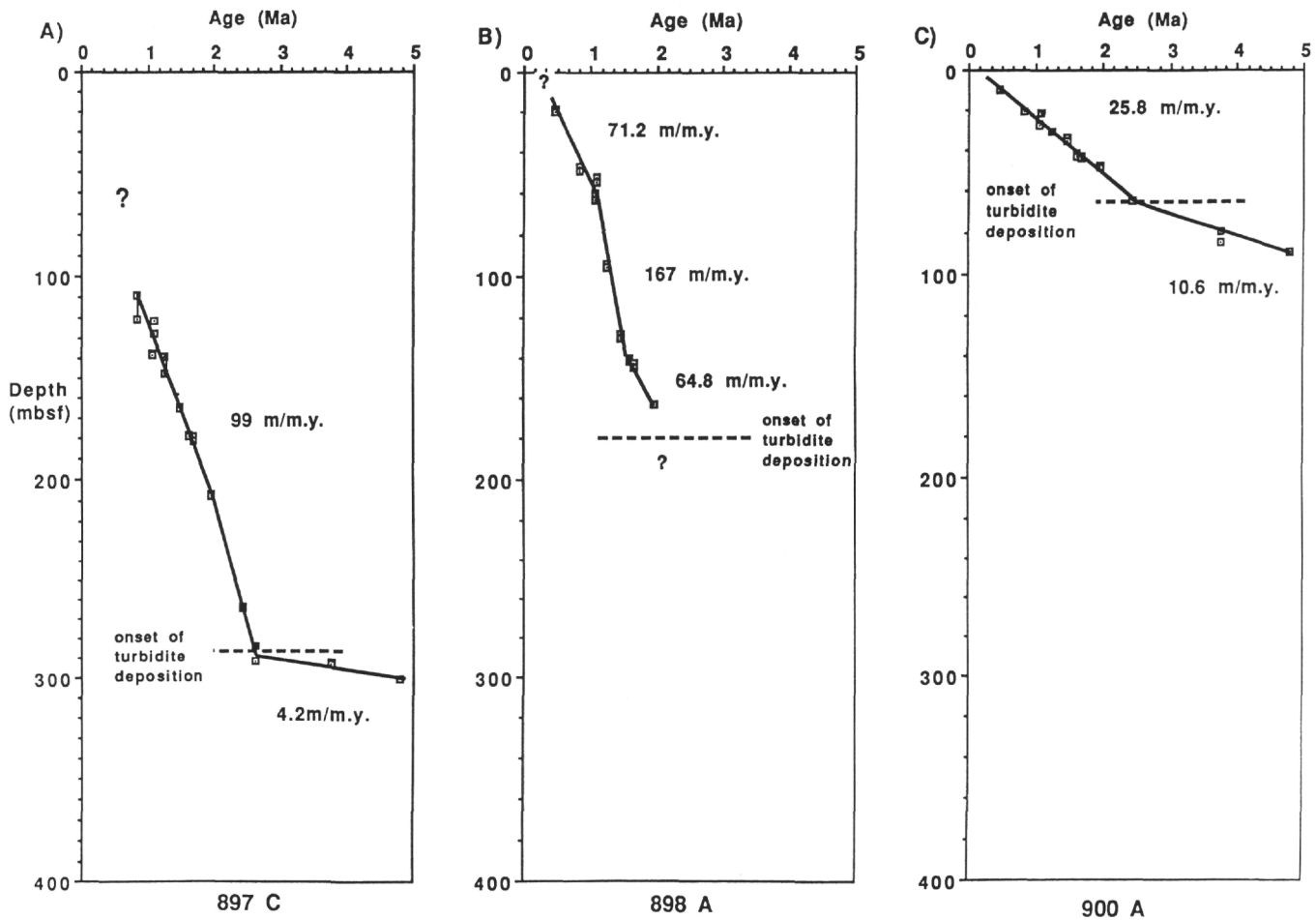
Figure 16. Variations in rates of total sediment accumulation through time and across the margin. **A.** Age vs. depth plot of total sediment accumulation at Hole 897C. **B.** Age vs. depth plot of total sediment accumulation at Hole 898A. **C.** Age vs. depth plot of total sediment accumulation at Hole 900A (from Milkert et al., this volume).
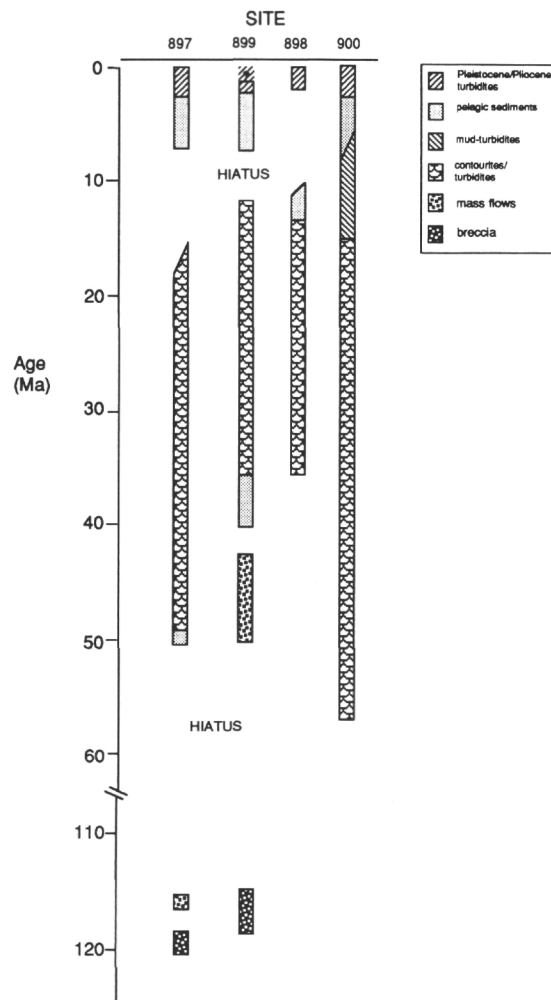
Figure 17. Summary of Cretaceous to Pleistocene sedimentation at Sites 897, 898, 899, and 900.